Lithos 366–367 (2020) 105569

Contents lists available at ScienceDirect

Lithos

journal homepage: www.elsevier.com/locate/lithos

Research Article

Cadomian Magmatic Rocks from Zarand (SE Iran) Formed in a Retro-Arc Basin

Fatemeh Sepidbar [a,b,*], Hadi Shafaii Moghadam [a,c], Congying Li [d], Robert J. Stern [e], Peng Jiantang [f], Yusef Vesali [g]

[a] School of Earth Sciences, Damghan University, Damghan 36716-41167, Iran
[b] State Key Laboratory of Geological Processes and Mineral Resources, School of Earth Sciences, China University of Geoscience, Wuhan 430047, China
[c] FB4–Dynamics of the Ocean Floor, GEOMAR, Helmholtz-Zentrum für Ozeanforschung Kiel, Wischhofstr. 1-3, 24148 Kiel, Germany
[d] Key Laboratory of Mineralogy and Metallogeny, Guangzhou Institute of Geochemistry, Chinese Academy of Sciences, Guangzhou 510640, China
[e] Geosciences Dept, University of Texas at Dallas, Richardson, TX 75083-0688, USA
[f] State Key Laboratory of Ore Deposit Geochemistry, Institute of Geochemistry, Chinese Academy of Sciences, Guiyang 550002, Guizhou, China
[g] Department of Geology, Faculty of Sciences, University of Tehran, Tehran 14155-64155, Iran

ARTICLE INFO

Article history:
Received 15 December 2019
Received in revised form 3 May 2020
Accepted 4 May 2020
Available online 11 May 2020

Keywords:
Cadomian magmatism
Retro-arc basin
Alkaline rocks
Zircon U-Pb
Iran

ABSTRACT

A major arc-related magmatic episode is recorded in the Ediacaran-Early Cambrian (Cadomian) crust of Iran and Anatolia due to the southward subduction of Prototethyan oceanic lithosphere beneath N Gondwana. This magmatism was generated at a convergent margin, fragments of which can be traced for thousands of kilometres, from west Avalonia to the Lhasa terrane. Cadomian crustal tracts in Iran and Tauride-Anatolia are represented by abundant arc-like plutonic and volcanic rocks and a series of retro-arc, rifted basins dominated by thick sequences of terrigenous rocks as well as both calc-alkaline and alkaline magmatic rocks. This paper presents new zircon U-Pb as well as geochemical-isotopic data from plutonic (granite to gabbro) and volcanic (basalt to rhyolite) magmatic rocks of a Cadomian retro-arc rifted basin from Zarand in SE Iran. Geochemical data indicate two different geochemical signatures; high K calc-alkaline-shoshonitic, characterized by strong depletions in Nb, Ta, P, Ti, and alkaline rocks (and A_1-type intrusions), with strong OIB-like trace element patterns. Cadomian OIB-like rocks- as well as A_1-type intrusions- are rare in the basements of Iran and Anatolia and are only documented as minor gabbroic intrusions and/or (meta-) volcanic rocks from Saghand (central Iran), NE Iran and from exotic blocks from Ediacaran salt domes. Moreover, A_2-type granites are also present in the Cadomian crust of Iran. Zarand volcanic rocks are interlayered with Rizu-Dezu terrigenous sedimentary rocks, whereas plutonic rocks intruded these metasediments. New zircon U-Pb ages show that high K calc-alkaline-shoshonitic rocks formed ~ 537-536 Ma, whereas A_1-type granites crystallized at ~535 Ma. Most zircons from A_1-type granites show positive $\varepsilon Hf(t)$ values from +1.1 to +5.1, mostly higher than high K calc-alkaline-shoshonitic rocks with $\varepsilon Hf(t)$ between −6.6 and +8.1. Bulk rock Nd-Sr isotopic data (e.g., $\varepsilon Nd(t) = +0.3$ to +4.0) for OIB-like rocks confirm that these rocks originated from an enriched OIB-like mantle source, whereas high K calc-alkaline-shoshonitic rocks (with $\varepsilon Nd(t) = -7.7$ to −6.2) show strong interaction with, and/or re-melting of a continental crust. Our results are consistent with an interpretation that the Zarand volcanic-plutonic rocks as well as associated thick sequences of sedimentary strata rocks formed in a retro-arc rifted basin behind the Cadomian magmatic arc. This basin seems to have developed during the Ediacaran at ~570-560 Ma with deposition of Ediacaran Morad to Lower Cambrian Rizu-Dezo sedimentary rocks. The retro-arc extensional basin seems to have become magmatically active at 540-535 Ma, as shown by the occurrence of both high K calc-alkaline- shoshonitic and OIB-like magmatic rocks. This basin was flanked by a cratonic hinterland towards Gondwana and a magmatic arc to the N. The cratonic hinterland fed detritus with detrital zircons older than 0.6 Ga into the basin, whereas the magmatic arc shed detritus with 500-600 Ma old zircons. Our compiled and new data from Ediacaran-Early Paleozoic magmatic rocks also show that Cadomian high magmatic fluxes occurred differently in parts of Iran-Anatolia, with overlaps in some areas.

1. Introduction

The geochronological evolution, paleo-positions and mechanisms involved in the growth and reworking of the Phanerozoic supercontinents and adjoining continental blocks have been a matter of debate

* Corresponding author at: School of Earth Sciences, Damghan University, Damghan 36716-41167, Iran.
E-mail address: fatemeh_sepidbar@yahoo.com (F. Sepidbar).

https://doi.org/10.1016/j.lithos.2020.105569
0024-4937/

for many years. The Middle East is a good example of Phanerozoic crustal growth and consists of a complex mosaic of continental blocks that formed between Gondwana and Eurasia to the S and N, respectively (Ruban et al., 2007). These continental blocks make up most of the crust of the Caucasus (Armenia, Azerbaijan, Georgia and southwest Russia), Turkey, Iran, Afghanistan and the Tibetan plateau. They are variably deformed and occur within a wide tectonic belt between the Eurasian, Arabian and Indian plates. These blocks record several pulses of magmatism and both tectonic extension and shortening throughout the Phanerozoic. However, basement rocks and associated metasedimentary cover suggests that all of these terranes shared an analogous tectono-magmatic heritage, dating from Late Ediacaran and Early Cambrian. These terranes were affected by processes accompanying opening of the Paleotethys and Neotethys oceans and henceforth the evolution of the Hun (or Hunic including Turan, Tarim, N China, Annamia and Armorica-Sakarya) and Cimmerian terranes (including Lhasa, Anatolia, Iran and Afghan blocks) (e.g. (Cocks and Torsvik, 2002; Stampfli, 1996; von Raumer, 1998; von Raumer et al., 2002; von Raumer et al., 2003; von Raumer et al., 2015)). Iran and Anatolia are commonly regarded as Cimmerian blocks since they are floored by Cadomian rocks (Kroner and Sengor, 1990; Sengor et al., 1991), although (Tauride-) Anatolia seems to have behaved differently- as a distinct continental block- detached from Gondwana during Early Triassic and accreted to Laurasia in Late Cretaceous (Topuz et al., 2013; Topuz et al., 2020).

The igneous rocks and sediments generated during Ediacaran-Early Cambrian, referred to as Cadomian (Crowley et al., 2000), make up much of the crust of western Europe although some western segments are called Avalonian. Cadomian and Avalonian crust now underlie large tracts of eastern N America and southern Europe (Linnemann et al., 2011). Cadomian crust can be traced eastwards into SE Europe, Taurides-Anatolide, and Iran and perhaps further into Central Asia (von Raumer et al., 2002). Cadomian-Avalonian fragments formed on the northern margin of Greater Gondwana and rifted away from Gondwana first in Early Paleozoic (such as Turan, Tarim etc.) and then in Late Paleozoic-Early Mesozoic (such as Iran, Tauride-Anatolia) during both opening of the Rheic or Paleotethys and Neotethys Oceans, respectively (Nance et al., 2002).

It is suggested that the Cadomian magmatic rocks on the northeastern margin of Gondwanaland formed at an active continental margin on the northern flank of the Arabian-Nubian Shield (ANS; (Garfunkel, 2015; Stern, 1994) and older crust to the west. ANS tectono-magmatic evolution began ~850 Ma as intraoceanic convergent margins and ended at 570 Ma as colliding blocks of E and W Gondwana cratonized along the East African Orogen (-EAO). The Cadomian convergent margin trended along the northern margin of Greater Gondwanaland, perpendicular to the EAO, indicating reorganization of global plate boundaries ~600-550 Ma. Cadomian crust formation in Iran and Anatolia began ~620 Ma and ended ~500 Ma, although most igneous activity occurred between 530 and 570 Ma. Arc to back-arc basin activity led to the Early Paleozoic rifting of Gondwana at ~530 to 485 Ma to open the Rheic ocean (Nance et al., 2010; Sanchez-Garcia et al., 2008), whereas Cimmerian blocks are suggested to have accreted to S Eurasia as the result of the opening of the Neo-Tethys Ocean during the Permian-Early Triassic (Moghadam et al., 2015) and/or closure of Neotethyan Ocean in Late Mesozoic (Topuz et al., 2013). Previous studies have established that Cadomian magmatic rocks formed due to subduction of the Proto-Tethys Ocean beneath the northern margin of Gondwana. Taurides-Anatolia and Iran seem to be part of a single contiguous orogenic plateau consisting of allochthonous Gondwanan continental crust with 620-500 Ma Cadomian magmatic and meta-igneous basement rocks (Moghadam et al., 2015; Moghadam et al., 2017a). Geochronological and geochemical data from Anatolia and Iran indicate that Cadomian subduction-related magmatism initiated at 620 Ma and finished at 500 Ma (e.g., (Hassanzadeh et al., 2008; Honarmand et al., 2018a; Moghadam et al., 2017a)), but crustal extension and its accompanying magmatic "flare-up" started at ~572 Ma and ended at ~528 Ma, lasting for ~44 Myr (Moghadam et al., 2017c).

Cadomian magmatic rocks in most exposures from NW-, NE and central Iran include metagabbroic rocks, orthogneisses and metagranitoids, which grade upward into volcanic rocks, mostly with felsic composition (Hassanzadeh et al., 2008; Moghadam et al., 2015). Basaltic rocks are rare. Cadomian intrusive rocks intruded mostly into metasediments including paragneisses and amphibolites. Zircon U-Pb ages from these magmatic rocks reveal Late Neoproterozoic-Early Cambrian ages, from ~620 Ma to ~500 Ma (Faramarzi et al., 2015; Hassanzadeh et al., 2008; Horton et al., 2008; Hosseini et al., 2015; Moghadam et al., 2015; Rahmati-Ilkhchi et al., 2011; Ramezani and Tucker, 2003). However, the timescale of magmatism in this prolonged continental arc construction seem to be different in various parts of Iran. Late Paleozoic rifting of the Cadomian magmatic arc from Gondwana further complicates efforts to reconstruct the magmatic architecture of the Cadomian continental arc of Iran, especially the position of the magmatic front *vs* retro-arc regions. However, it seems that some exposures from SE Iran which include Ediacaran to Late Cambrian sediments, with minor volcanic rocks and few intrusions, might represent retro-arc or back-arc regions. These sediments have abundant Archean as well as Neoproterozoic detrital zircons. In contrast, magmatic-front areas are characterized by metasediments pierced by abundant Cadomian intrusions like exposures in NW and NE Iran. These sediments from the magmatic front areas are interpreted to have been deposited in intra-arc basins which were mostly (>90%) filled with detritus derived from erosion of local Cadomian rocks, as shown by detrital zircons in metasediments from NE and NW Iran (Balaghi et al., 2014; Honarmand et al., 2018a). The minimum age of sedimentation is variable and overlaps in time with magmatic activity.

In this study we present new whole rock geochemical and Sr-Nd-Pb isotope data, zircon U-Pb ages and Lu-Hf isotope for Cadomian magmatic rocks from Zarand (SE Iran). We believe this area is a retro-arc fragment of the Cadomian magmatic arc from N Gondwana. Retro-arc basins occur on the overlying plate of subduction systems and situated behind the main magmatic arc (Li et al., 2018). Furthermore, we use these new data and other compiled data from other Iranian outcrops to constrain the paleogeography and geodynamic setting of the Cadomian continental arcs in Iran and Anatolia.

2. Geological background

The Cadomian peripheral accretionary margin and related magmatism reflected south-dipping subduction of Prototethys oceanic lithosphere beneath northern Gondwana (Linnemann et al., 2008; Linnemann et al., 2014; Pereira et al., 2006), leading to widespread extension (back-arc and retro-arc basins) within Anatolia and Iran. Documented Cadomian exposures in Turkey are found in the south (Poturge massif), the west (Menderes and Sandikli massifs) and the NW (Istanbul zone). In Iran, Cadomian exposures are documented from regions in western (Golpayegan), northwestern (Khoy-Salmas, Zanjan-Takab), northeastern (Torud, Taknar), northern (Lahijan granites), and central Iran (Saghand) (Hassanzadeh et al., 2008) (Fig. 1). Most Cadomian felsic magmatic rocks from Iran and Anatolia have "volcanic arc granite" (VAG) geochemical signatures and within plate granites (WPG) are rare (Badr et al., 2013; Balaghi et al., 2014; Rossetti et al., 2015). Based on zircon Hf and whole-rock Nd isotopic compositions, it is supposed that these magmas formed during partial melting of older continental crust (Paleoproterozoic - Archean) or by mixing between juvenile mantle derived-melts and old continental crust, during the subduction of the Prototethyan Ocean beneath northern Gondwana (Abbo et al., 2015; Moghadam et al., 2015; Moghadam et al., 2017a). Cadomian within plate-like, alkaline felsic rocks are rare but occur in some places in NW and central Iran and as exotic blocks within Ediacaran salt domes from S Iran and are dominated by rhyolitic lavas. These felsic volcanic rocks and their intrusive equivalents are known as Zarigan-Narigan units in

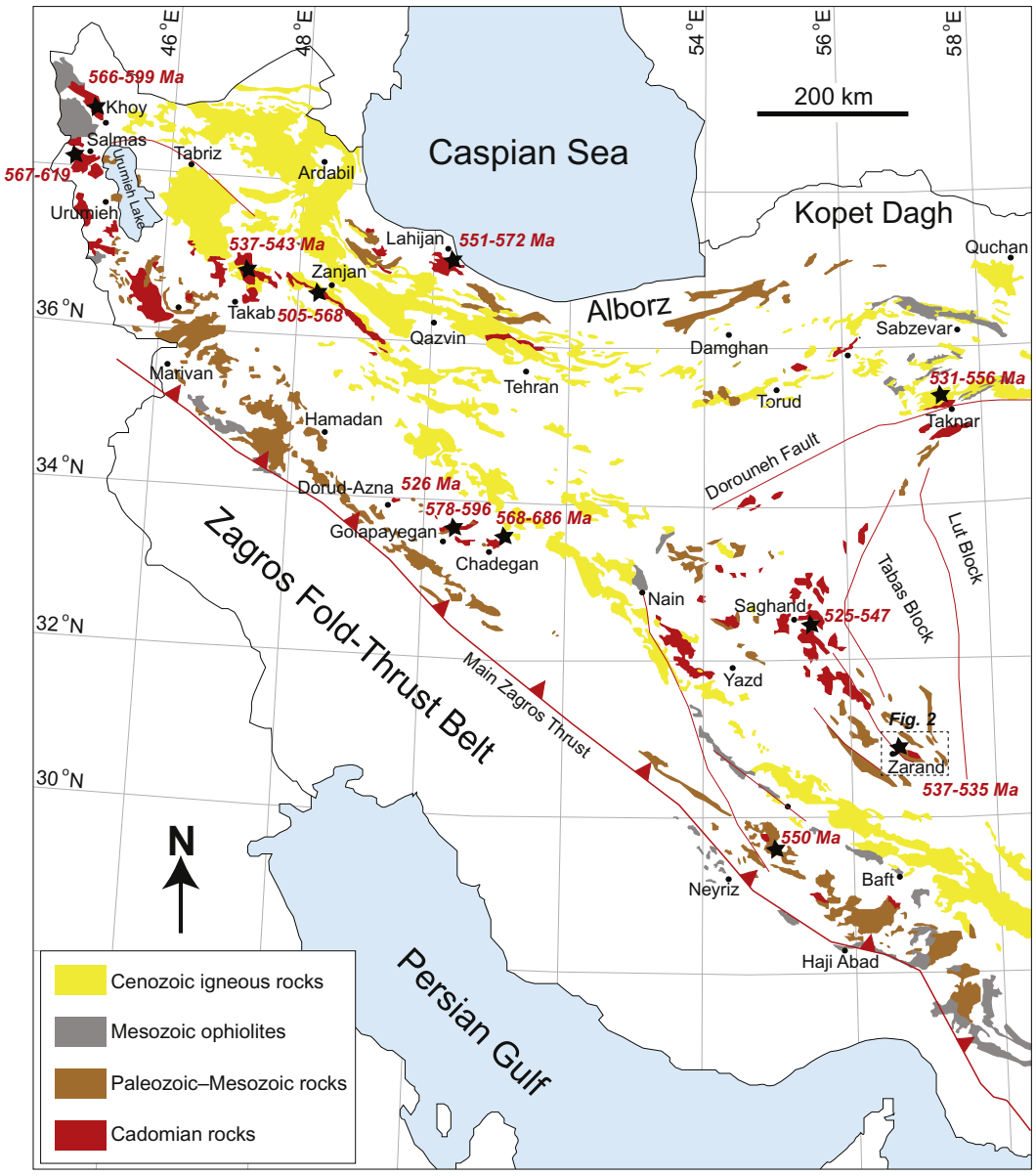

Fig. 1. Simplified geological map of Iran showing the distribution of Cadomian basement rocks, Paleozoic-Mesozoic volcano-sedimentary rocks, Cenozoic igneous rocks and Paleozoic-Mesozoic ophiolites.

central Iran, Qare-Dash rhyolites in NW Iran and Hormoz rhyolites in S Iran exotic blocks. There are different scenarios suggested for the genesis of these felsic rocks including; 1- Formation in an intra-plate rift setting (Momenzadeh and Heidari, 1995); 2- Formation above a subduction zone (for central Iran Zarigan-Narigan rhyolites and their intrusive equivalents; (Ramezani and Tucker, 2003); 3- Submarine volcanism in an extensional back-arc for Hormoz rhyolites (Faramarzi et al., 2015); 4- Generation in fault-bounded trough basins during Gondwana rifting (Berberian and King, 1981; Talbot et al., 2009); and 5 Formation in a continental, intra-plate rift (Atapour and Aftabi, 2017a; Atapour and Aftabi, 2017b).

Alkaline felsic to mafic intrusive rocks are also present and range from alkali-feldspar granites to kaersutite-bearing amphibole gabbros. These intruded Late Neoproterozoic metamorphic rocks and Early Cambrian volcano-sediments, for example those from Saghand (Ramezani and Tucker, 2003) (Fig. 1). In addition, alkaline basalts and metabasalts (with metagabbros) are rare but occur in NE and Central Iran (Balaghi et al., 2010; Maleki et al., 2019; Veiskarami et al., 2019). Zircon U-Pb dating of alkaline Zarigan rhyolites (Saghand) yielded an $^{206}Pb/^{238}U$ age of 526 ± 3 Ma (Ramezani and Tucker, 2003). In addition, Cadomian alkali-feldspar granites or A-type granites and orthogneisses have reported from Sanandaj-Sirjan Zone of Iran (e.g., near Ghaleh-Dezh and in Azna-Dorud). These intrusive rocks are geochemically classified as A_2-type granites (with crustal Nd isotope signatures; εNd(t)= −1.2 to −1.5) and have zircon U-Pb ages of 568 ±11 Ma (Shakerardakani et al., 2015) and 525.6 ±4 Ma (Shabanian et al., 2018).

Zarand magmatic rocks in SE Iran occupy an area of ~50 km^2 (Fig. 2). The oldest sediments in this area include Ediacaran sandstones and shales of the Morad series (Fig. 2A). The Ediacaran age for the Morad rocks was suggested based on radiometric dating, stratigraphic position and distinct Ediacaran and Cambrian fauna (Horton et al., 2008; Ramezani and Tucker, 2003). The Morad formation is found in SE Iran, but its stratigraphic equivalents such as the Tashk and Kahar Formations, have been reported from central Iran (Saghand) as well as N Iran, respectively (Etemad-Saeed et al., 2015; Ramezani and Tucker, 2003). Cadomian clastic rocks of the Rizu-Dezu Formation rest over

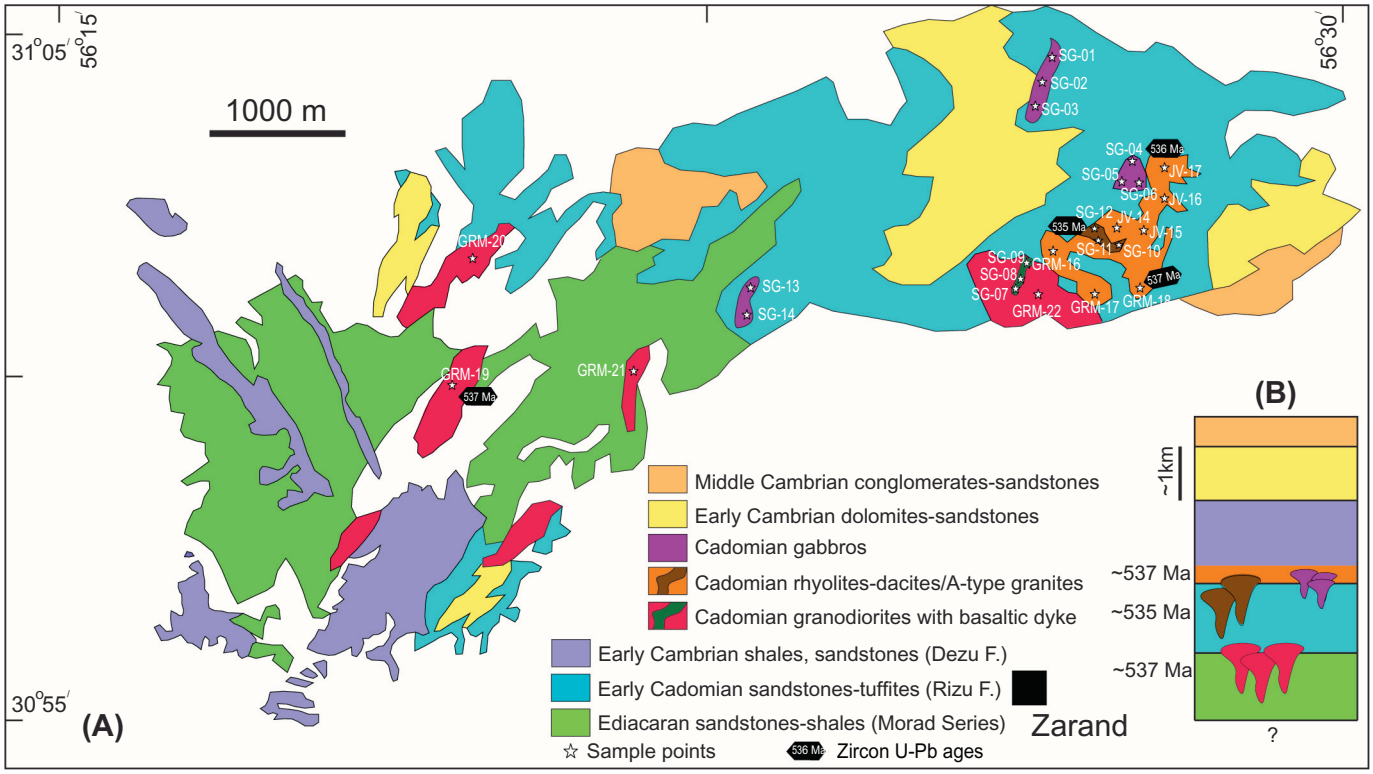

Fig. 2. (A) Simplified geological map of the Zarand area (modified after Jalal Abad 1/100000 map, Geological Survey of Iran). (B) Schematic lithological column showing the relationships between Zarand rock units and new zircon U-Pb ages obtained during this study.

the Morad series (Fig. 2B). A U-Pb zircon age of 528.2 ±0.8 Ma for basal dacites from the Rizu-Dezu Formation confirms an Early Cambrian age (Horton et al., 2008; Ramezani and Tucker, 2003). The Rizu-Dezu Formation has two units; (I) a lower unit of grey, green to pink greywackes and (II) an upper thick (>1100 m) volcano-sedimentary unit of siltstones, tuffaceous sandstones, thick iron-rich layers, tuffites, intermediate to felsic volcanic rocks, tuffaceous limestones and conglomerates (Fig. 2). Felsic volcanic rocks include dacite, rhyolites, ignimbrites and other pyroclastics. Dacite lava flows occur in the eastern and southern part of region. Small (few 100m across) intrusions of A-type granite to granodiorite are injected into the Rizu - Dezu volcano-sedimentary unit. Granodiorites are also exposed as small stocks in the southwest of the Zarand region. Field observations show that granodiorites crosscut both Ediacaran Morad series and Early Cambrian sedimentary rocks of the Rizu-Dezu Formation. Locally, granodiorites intrude green tuffs. A-type granites are also injected into the Rizu-Dezu Formation. Subvolcanic mafic to intermediate rocks occur both as small stocks and dikes or sills. These rocks crosscut Early Cambrian sedimentary rocks of the Rizu-Dezu Formation.

3. Sample description and petrography

Petrographically, Zarand magmatic rocks are subdivided into dacites, rhyolites, granodiorites, A-type granites, alkaline gabbros and basalts. The petrography of these lithologies is discussed further below. Dacites show aphyric to porphyritic textures. They contain quartz and plagioclase phenocrysts set in a microcrystalline to cryptocrystalline groundmass consisting of quartz and intergrowths of sodic plagioclase and K-feldspar. Biotite, titanite and iron oxides occur as accessory minerals. Quartz with resorbed texture is the main phenocryst (~47% volume). Plagioclase is altered into epidote and calcite whereas alkali feldspars are altered to sericite. Apatite, biotite and iron oxides are accessory minerals while calcite, sericite, titanite, hematite and chlorite are common secondary minerals. Rhyolites are less abundant than dacites and occur as lava flows. They have porphyritic textures and contain phenocrysts of biotite (5-7%), sanidine (~5-10%), and quartz (20%) set in a cryptocrystalline-felsite groundmass.

Granodiorite stocks occur in the eastern and western Zarand area (Fig. 2). They show porphyritic to granular texture and contain euhedral to subhedral phenocrysts of quartz (30%), K-feldspar (25%), plagioclase (35%), amphibole and biotite (3-8%). Subhedral to anhedral K-feldspar (0.5-2 mm) are perthitic. K-feldspar is usually anhedral, occurs interstitially between plagioclase grains and is partially replaced with clay minerals. Magnetite, ilmenite, zircon and apatite are accessory minerals. Mafic minerals are replaced by secondary minerals such as chlorite and calcite. Tabular plagioclase varies from 0.5 to 3 mm in size.

A-type granites occur as shallow intrusions. These rocks contain quartz, K-feldspar and minor sodic plagioclase (albite). Chloritized amphiboles are also common.

Alkaline gabbros have plagioclase (50-60 wt. %), high-Ti brown amphibole (20-30 wt. %) and clinopyroxene (5-10 wt. %) as primary constituents, although minor olivine and biotite can be observed in some samples. Epidote, clinozoisite and chlorite are secondary minerals. These rocks are generally medium grained with a granular texture. Clinopyroxenes are altered into amphiboles in some samples. Plagioclase is altered into scapolite and albite.

Basaltic dikes are generally fine-grained with intersertal textures. The main constituents are plagioclase and altered clinopyroxene, whereas the accessory minerals consist of opaque minerals, apatite and biotite. Epidote, chlorite, calcite and albite are common secondary minerals.

4. Results

4.1. Geochronology

We determined U-Pb zircon ages for four samples using the LA-ICPMS method: one A-type granite, one granodiorite, one dacite and

one rhyolite. These results are discussed below. Detailed analytical procedures are described in Appendix A.

4.2. A-type granite

We analyzed one sample of A-type granite (sample SG-12) for zircon U-Pb ages (Table S1). Cathodoluminescence (CL-) images (Fig. 3A) show the position of the laser spots and the U-Pb age of the representative zircons. Zircons from sample SG-12 are subhedral to euhedral and show oscillatory zonation (Fig. 3A). U, and Th contents range from 207 to 451 ppm and 82 to 319 ppm, respectively. The Th/U ratio changes from 0.4 to 0.9 which is typical for zircons from intermediate igneous rocks (Belousova et al., 2002). Twenty-five analyzed zircon from alkaline granite yielded a concordia age of 535.2 ± 1.4 Ma (MSWD=0.8) (Fig. 4A).

4.3. Granodiorite

Thirty zircon grains from granodiorite sample GRM-19 were analyzed for U-Pb ages (Table S1). Some zircons show inherited cores (Fig. 3B). U and Th contents of zircons vary from 132 to 754 and 77 to 680 ppm, respectively. Th/U ratios range from 0.4 to 1.0, which are typical for magmatic zircons (Belousova et al., 2002). Zircons from sample GRM-19 yielded a concordia age of 537.2 ± 2.4 Ma (MSWD=2.4) (Fig. 4B), which is interpreted as the crystallization age of this granodiorite. Three zircon cores show $^{207}Pb/^{206}Pb$ ages of 1184.9 ± 55, 1865.7 ± 52 to 2083.6 ± 22 Ma, which are interpreted as the age of some crustal protolith.

4.4. Dacite and rhyolite

Zircons in dacite sample GRM-18 and rhyolite JV-17 show oscillatory zoning (Fig. 3C and D). samples GRM-18 (dacite) has low U (109-305ppm) and Th (58-185 ppm) contents and their Th/U ratios vary from 0.4 to 0.7. Twenty-four analyses from this sample yielded an age of 535.5 ± 1.6 Ma (MSWD=0.77) (Fig. 4C) which is interpreted as the crystallization age of dacitic sample GRM-18. One $^{207}Pb/^{206}Pb$ age on zircon cores is 2346 ± 28 Ma.

Zircons from rhyolite sample JV-17 range from 100 to 200μm long, with length to width ratios between 1:1 and 2:1. Zircons are mostly euhedral and show oscillatory zoning (Fig. 3D). Twenty analyzed zircons show low to moderate U (157-1977 ppm) and Th (67-1139 ppm) contents and narrow Th/U ratios of 0.4 to 0.6. A concordia age from twenty-three analyses of this sample yielded is 536.5 ± 1.7 Ma (MSWD=0.9) (Fig. 4D) which is interpreted as the crystallization age of this rhyolite.

4.5. Whole rock geochemistry

Major, trace and rare earth element contents of Cadomian magmatic rocks from the Zarand region are given in Table S2. Detailed analytical procedures are described in Appendix A. Zarand Cadomian igneous rocks can be subdivided into two distinct suites: 1) high-K calc-alkaline and shoshonitic rocks and 2) Alkaline mafic rocks and granites. Data for these are discussed separately below.

4.6. Zarand high-K calc-alkaline and shoshonitic rocks

Zarand granodiorites and dacites/rhyolites show subalkaline signatures on the Na_2O+K_2O *vs* SiO_2 diagram of (Winchester and Floyd, 1977) (Fig. 5A). Dacites have high SiO_2 (68.7-72.9 wt. %) and Zr/Ti ratios (0.16-0.23). MgO and Al_2O_3 content of dacites/rhyolites range from 0.59 to 1.95 *wt%* and 12.25 to 15.23 *wt%*, respectively. A/CNK (molar $Al_2O_3/(CaO+Na_2O+K_2O)$ ratio of these rocks varies 1.45-2.03, displaying a peraluminous signature (Fig. 5B). Granodiorites have similar SiO_2 (68.6-71.2 *wt%*) and MgO and Al_2O_3 contents range from 0.55 to 1.75 *wt%* and 12.98 to 14.53 *wt%*, respectively. The A/CNK ratio of these rocks varies in the range of 1.4-1.9, showing a peraluminous signature (Fig. 5B). Both granodiorites and dacites have high-K_2O content and are similar to high-K calc-alkaline rocks and shoshonites (Fig. 5C). These samples are similar to volcanic arc granites (Fig. 5D).

Chondrite-normalized rare earth element (REE) patterns of granodiorites and dacites/rhyolites (Figs. 6A-C) show high $La_{(n)}/Yb_{(n)}$ ratio of 6.04-14.25, with conspicuous negative Eu anomalies (Eu/Eu^*= 0.44 to 0.89). On a multi-element, N-MORN-normalized diagram (Figs. 6B-D), these rocks exhibit positive anomalies for Rb, Ba, Th, U, K, Pb and negative anomalies in Ti, Sr, P and Nb relative to N-MORB. The geochemical signatures of granodiorites and dacites, including depletion in Nb, Ti and enrichment in large-ion lithophile elements (LILEs) and high ratios of light rare elements (LREEs)/heavy rare earth elements (HREEs), are similar to the geochemical characteristics of continental arc magmatic rocks (Ducea et al., 2010). Granodiorite and dacites/rhyolites have so many features in common (including their age), they may be intrusive and extrusive expressions of the same magma.

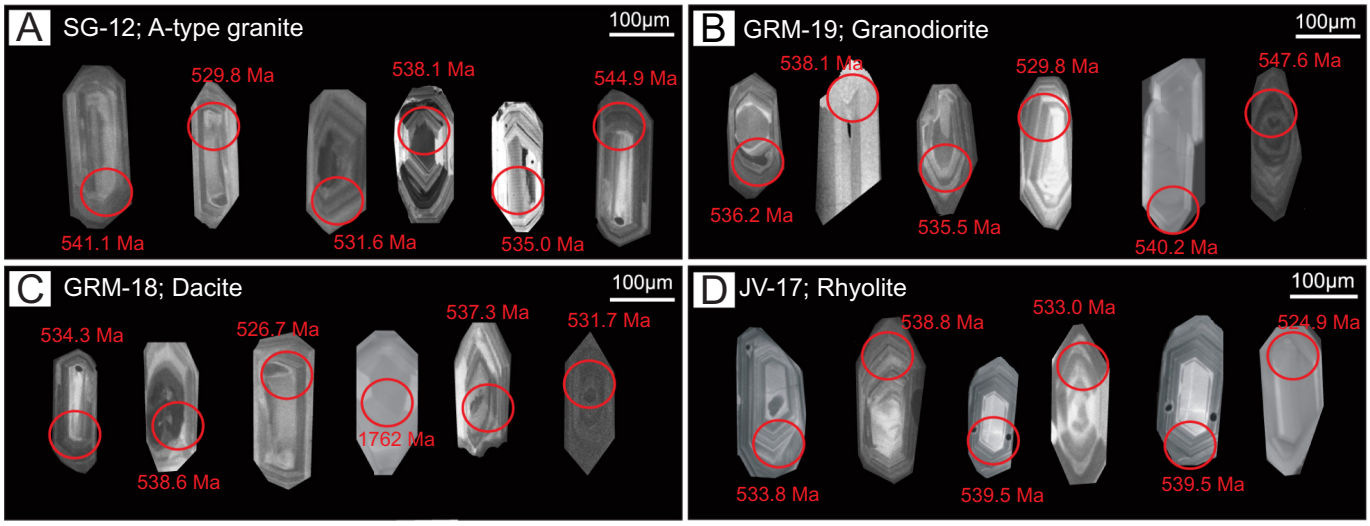

Fig. 3. Cathodoluminescence images of zircon grains from the Cadomian magmatic rocks of Zarand. Red circles show analytical spots for U-Pb and Hf isotopes, respectively.

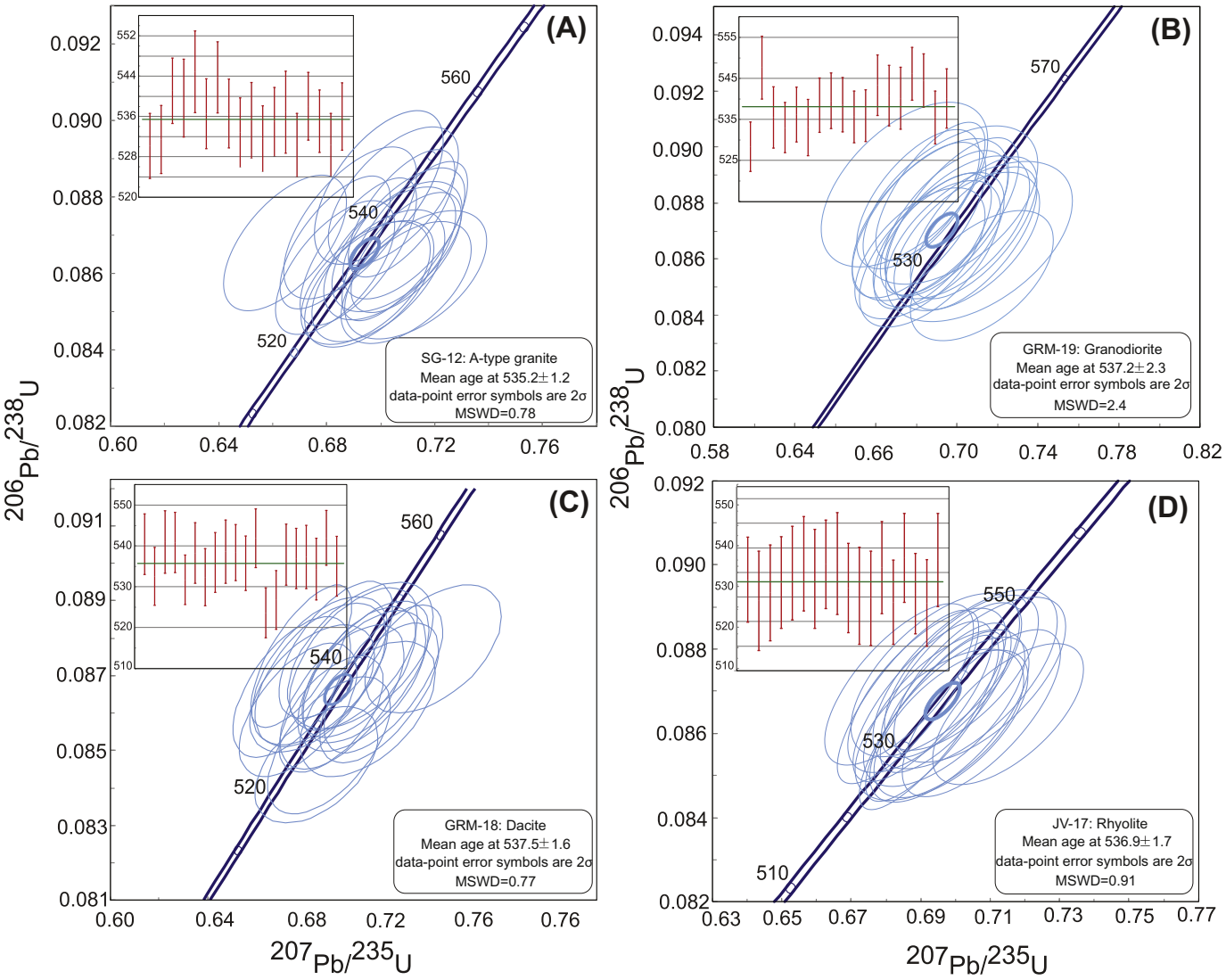

Fig. 4. Concordia and weighted mean $^{206}Pb/^{238}U$ age plots for the investigated zircons from the Late Neoproterozoic-Cambrian Zarand magmatic rocks.

4.7. Zarand alkaline rocks

Zarand basalts, gabbros and A-type granites show high content of alkalies (Na_2O+K_2O) and some other alkaline characteristics. Basalts show narrow ranges of SiO_2 (47.2- 49.4 *wt%*), high concentrations of Al_2O_3 (16.40-17.30 *wt%*), and K_2O (2.1-2.2 *wt%*) and moderate contents of TiO_2 (1.12 to 1.45 *wt%*) and Na_2O (2.80 to 3.40 *wt%*). Gabbros have lower SiO_2 (43.07-47.13 *wt%*) and Al_2O_3 (14.5-16.9 *wt%*) compared to basalts. These rocks are characterized by variable K_2O (0.80 to 2.98 *wt%*) but high Na_2O (4.12 to 5.56 *wt%*) contents. A-type granites are characterized by 72.70 to 75.20 *wt%* SiO_2, 11.20-13.10 *wt%* Al_2O_3, 4.7-5.8 *wt%* K_2O, 3.7-5.2 *wt%* Na_2O, and 0.96-1.23 Na_2O/K_2O ratio. The A/CNK ratio for A-type granites ranges from 1.18 to 1.24, displaying peraluminous signatures (Fig. 5B). Alkaline mafic igneous rocks are enriched in Na_2O, with K_2O/Na_2O <1 and plot in the trachy-basalt to tephrite and within-plate fields in SiO_2 *vs* Na_2O+K_2O and Y+Nb *vs* Rb diagrams, respectively (Fig. 5C-D). Chondrite-normalized rare earth element (REE) patterns of basalts show enrichment in LREEs relative to HREEs, with $La_{(n)}/Yb_{(n)}$ ratio of 18.2 to 9.2 and without Eu anomalies ($Eu/Eu^* = 1.03$-1.12) (Fig. 6E). In a N-MORB-normalized multi-element diagram (Sun and McDonough, 1989), LILEs such as K, Ba, Rb, Th and U are enriched relative to high-field strength elements (HFSEs) such as Nb, Ti and Zr (Fig. 6F). A-type granites and gabbros are also enriched in LREEs relative to HREEs, with $La_{(n)}/Yb_{(n)} = 13.2$ to 22.5 and 8.8 to 14.1, respectively. These rocks do not show Eu anomalies ($Eu/Eu^* = 0.97$-1.56) (Fig. 6G). On N-MORB normalized spider diagram (Fig. 6H), basalts, gabbros, and A-type granites show steep HREE to LREE - OIB-like trace element patterns with no HFSE depletions

4.8. Zircon Lu-Hf isotopes

The measured $^{176}Lu/^{177}Hf$ and $^{176}Hf/^{177}Hf$ ratios of zircons in Zarand igneous rocks are summarized in Table S3. Detailed analytical procedures are described in Appendix A. The $^{176}Hf/^{177}Hf$ ratios vary between 0.282331 to 0.282583 for the alkaline granites and 0.282250 to 0.282669 for high-K calc-alkaline to shoshonitic rocks (samples GRM-18, GRM-19 and JV-17), except one point with low $^{176}Hf/^{177}Hf$ ratio of 0.281551. Zircons from A-type granites have positive εHf(t) values of +1.1 to +5.1 (*av* +3) (Fig. 7A), except one point with negative εHf (t) value of −3.8, suggesting that nearly all zircons from A-type granites have juvenile signatures without significant contribution of crustal components in the melt source or during the melt ascent and emplacement. Crustal model ages of zircons from A-type granites are in the range of 0.9 to 1.3 Ga. Zircons from high-K calc-alkaline to shoshonitic rocks including granodiorites and dacitic-rhyolitic lavas have variable εHf(t) values of −6.6 to +8.1 (except one point with negative εHf

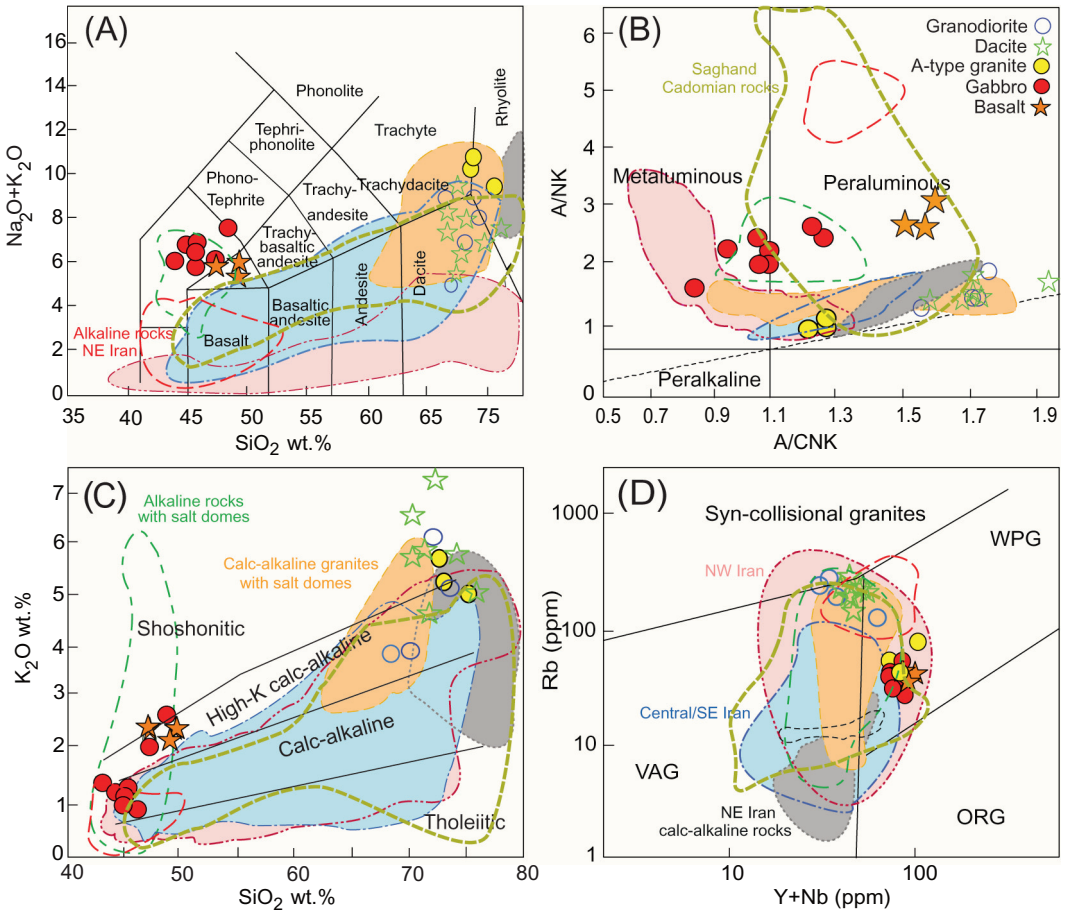

Fig. 5. Total alkalis versus SiO_2 diagram after (Lebas et al., 1986); (B) ANK (molar Al_2O_3/Na_2O+K_2O) *vs* A/CNK (molar $Al_2O_3/CaO+Na_2O+K_2O$) diagram; (C) SiO_2 *vs* K_2O diagram (Peccerillo and Taylor, 1975) and (D) Rb *vs*Y +Nb diagrams (Pearce et al., 1984) for classification of the Zarand Cadomian magmatic rocks. Data for Iran Cadomian rocks are from (Badr et al., 2013; Balaghi et al., 2014; Moghadam et al., 2015; Moghadam et al., 2016; Moghadam et al., 2017a). Bulk rock data for Cadomian exotic blocks within salt domes is from Asadi et al., (unpublished data). Data for NE and Central Iran alkaline mafic rocks are from (Balaghi et al., 2010; Maleki et al., 2019; Veiskarami et al., 2019), whereas data for Saghand rocks are from (Ramezani and Tucker, 2003).

(t) value of -31.4) (*av* +1.5), indicating that mantle-derived magmas and pre-existing crustal material were involved in their genesis. Crustal model ages of zircons from high-K calc-alkaline-shoshonitic rocks are in the range of 0.8 to 1.2 Ga, except one point with T^C_{DM} age of 2.4 Ga.

4.9. Bulk rock Sr-Nd-Pb isotopes

We analyzed 10 samples (2 A-type granites, 2 gabbros, 2 basalts, 2 granodiorites, 2 dacites) from Zarand Cadomian rocks for Sr-Nd-Pb isotopes (Table S4). Initial $^{87}Sr/^{86}Sr_{(i)}$, $^{143}Nd/^{144}Nd_{(i)}$, $^{206}Pb/^{204}Pb$ $^{207}Pb/^{204}Pb$ and $^{208}Pb/^{204}Pb$ of these rocks re-calculated based on their zircon U-Pb ages. The $^{87}Rb/^{86}Sr$ ration of Zarand alkaline rocks ranges from 0.349 to 0.385, 0.121 to 0.771 and 0.232 to 0.240 for A-type granites, gabbros and basalts, respectively. These rocks display initial εNd (t) values of +3.6 to +3.7 for the A-type granites, +3.8 to +4.0 for the gabbro, +0.3 to +3.1 for basalts. These rocks have depleted mantle model ages (T_{DM}) of ~0.8-1.1 Ga. Although $(^{87}Sr/^{86}Sr)_{(i)}$ values show considerable variations, from 0.7053 to 0.7111 for basalts, 0.7032 to 0.7033 for A-type granites and 0.6988 to 0.7049 for gabbro (Table S4), but they have positive εNd(*t*) values with narrow variations. Since, Nd isotopes are more resistant to alteration than Sr isotopes, it can be suggested that the Sr isotope has influenced by alteration for basalts relative to gabbro and A-type granites. Gabbros and A-type granites show more juvenile (mantle-derived) isotopic composition relative to basalts (Fig. 7B).

High-K calc-alkaline rocks and shoshonites have εNd(t) values of −7.7 to −7.4 and −6.7 to −6.2, respectively, with depleted mantle model ages (T_{DM}) of 1.5 to 1.6 Ga. The $^{87}Rb/^{86}Sr$ ratios for granodiorites, dacite and rhyolite show values of 0.58 to 0.60, 0.78 and 0.62, respectively, so significant correction for radiogenic growth of Sr isotopes is needed to determine initial values. These rocks have $(^{87}Sr/^{86}Sr)_{(i)}$ ratios of 0.7195-0.7235 and 0.7112 to 0.7139. These isotopic values attest to remelting of much older continental crust to generate these magmas. The $^{206}Pb/^{204}Pb$ and $^{208}Pb/^{204}Pb$ values of granodiorites and rhyolites are also high, ranging from 15.62 to 19.35 and 37.11 to 40.68, respectively (Table S4). These samples are also characterized by radiogenic $^{207}Pb/^{204}Pb$ ratios, ranging between 15.51 and 15.87. These rocks plot above the Northern Hemisphere Reference Line (NHRL; (Zindler and Hart, 1986)), in the $^{207}Pb/^{204}Pb$ and $^{208}Pb/^{204}Pb$ *vs* $^{206}Pb/^{204}Pb$ diagram (Fig. 7C and D) and their isotopic composition is similar to that of continental crust. The $^{206}Pb/^{204}Pb$ and $^{208}Pb/^{204}Pb$ ratios of alkaline rocks are lower than the high-K calc-alkaline suite and change from 16.96 to 18.89 and 36.36 to 39.24, respectively (Table S4). These samples are also characterized by elevated $^{207}Pb/^{204}Pb$ ratios, ranging between 15.14 and 15.87. They plot above the Northern Hemisphere Reference Line (NHRL; Hart (1984)), in $^{207}Pb/^{204}Pb$ and $^{208}Pb/^{204}Pb$ *vs* $^{206}Pb/^{204}Pb$ diagrams (Figs. 7C and D).

5. Discussion

Cadomian igneous and sedimentary rocks constitute the main rock units that formed on the northern margin of Gondwana although this crust is now found in a >5000 km long belt in Eastern N. America, Europe, (Avigad et al., 2016) Turkey, Iran and Tibet (Wang et al.,

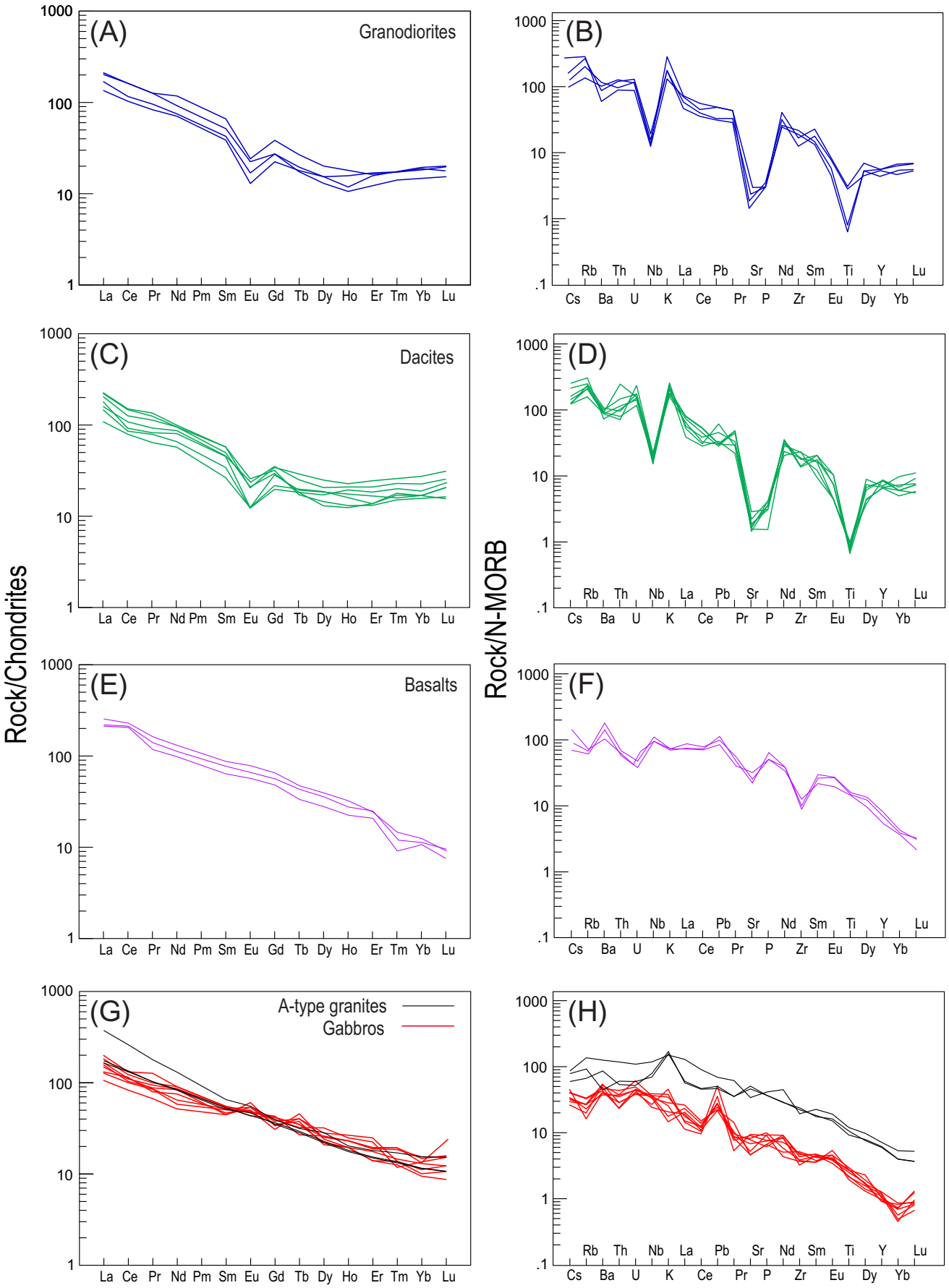

Fig. 6. Chondrite-normalized rare earth element (left) and N-MORB-normalized trace element patterns (right) for the Zarand Cadomian magmatic rocks. Chondrite and N-MORB normalized values are taken from (Sun and McDonough, 1989).

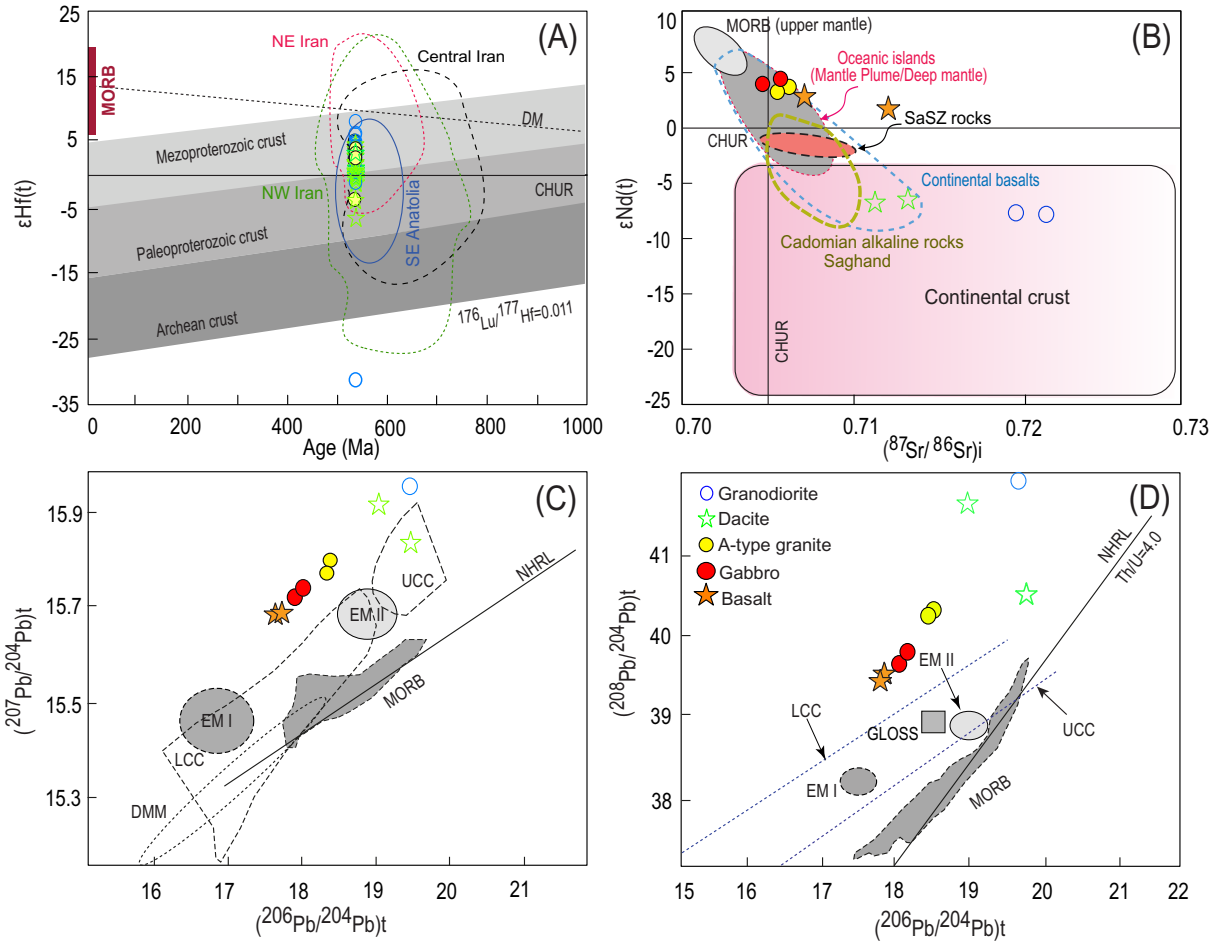

Fig. 7. (A) Initial Hf isotopic composition *vs* $^{206}Pb/^{238}U$ crystallization ages of the Zarand magmatic rocks. (B) εNd *vs* $^{87}Sr/^{86}Sr$, (C) $^{207}Pb/^{204}Pb$ *vs* $^{206}Pb/^{204}Pb$ and (D) $^{208}Pb/^{204}Pb$ *vs* $^{206}Pb/^{204}Pb$ diagrams for the Zarand Cadomian magmatic rocks. Mantle components including HIMU, EMI, EMII, DMM are from (Zindler and Hart, 1986); subduction-related, juvenile magmas and thick continental crust-derived rocks are from (Defant et al., 1992) and (Zhao et al., 2009), respectively. Bulk rock Nd and zircon Hf isotope data for Cadomian exotic blocks within salt domes is from Asadi et al., (unpublished data).

2016). Our results indicate that in addition to the high-K calc-alkaline-shoshonitic magmatism which characterized Cadomian arc igneous rocks, alkaline rocks are also present. These observations suggest that some Cadomian rocks in Iran formed in a back-arc region and/or retro-arc rifted basins behind (south of) the main magmatic arc. Below, we discuss the origin and petrogenesis of both Cadomian calc-alkaline and alkaline rocks separately. Then we will discuss the temporal and spatial occurrences of Cadomian rocks in Iran and Gondwana.

5.1. Petrogenesis of Cadomian high-K calc-alkaline-shoshonitic rocks

Zarand high-K calc-alkaline to shoshonitic magmatic rocks comprise granodiorites and dacites-rhyolites (~537-536 Ma) closely associated with alkaline stocks (~535 Ma). Granodiorites and dacites-rhyolites have geochemical characteristics that resemble I-type granites. They show geochemical similarities to continental magmatic arc-related rocks in the Th/Yb *vs* Ta/Yb diagram (Fig. 8A) (Tindle and Pearce, 1983). In addition, the Th/Ta ratio at relatively constant Yb values can be used to discriminate the tectonic setting of the analyzed samples as within-plate, active continental margin and oceanic arcs (Schandl and Gorton, 2002). The Th/Ta ratio of Zarand granodiorites and dacites-rhyolites range from 10.57 to 15.37 and 6.53 to 20.59, respectively and plot within the active continental margin arc field (Fig. 8B). The Zr/Nb *vs* Nb/Th diagram of (Condie, 2005b) (Fig. 8C) also suggests a magmatic-arc origin for the genesis of these rocks. Nearly all Cadomian rocks from NW, NE and Central Iran also have similarities to magmatic arc granites (Fig. 5D). Dacites-rhyolites and granodiorites belong to the high-K calc-alkaline/shoshonitic magmatic series and share their geochemical signatures both in terms of trace element patterns (Figs. 6A-D) and peraluminous characteristics (Fig. 5B). These rocks are cogenetic and may have formed from the same magma.

The high-K calc-alkaline to shoshonitic Zarand igneous rocks are characterized by enrichment in LREEs, Rb, Ba, Th, U, Pb and K, and depletion in Nb, Ta, Ti. These geochemical signatures are a feature of magmas erupted and emplaced in active continental arcs (Baier et al., 2008; Pearce and Peate, 1995). The noticeabley negative Nb-Ta anomalies may explained by a Nb-bearing phase during hydrous melting of the mantle wedge (Smedley, 1988) to generate the parental melts of these rocks. These rocks are also characterized by depletion in Sr and Eu, indicating plagioclase fractionation.

It is generally believed that high-K I-type felsic melts may be derived from melting of hydrous intermediate to mafic high-K meta-igneous rocks; i.e., melting of a heterogenous continental lower crust (e.g., (Roberts and Clemens, 1993; Sisson et al., 2014)) or form by mixing of mantle-derived magmas with crustal melts (e.g., (Hildreth et al., 1991; Huang et al., 2013)). Experimental data also confirm that partial melting of hydrous, calc-alkaline to high-K calc-alkaline, mafic to intermediate metamorphic rocks in the lower-middle crust can generate high-K, I-type felsic intrusions (Roberts and Clemens, 1993). Moreover, fractional crystallization (FC) of mantle-derived mafic magmas is an alternative mechanism for the generation of Zarand calc-alkaline-shoshonitic magmas. The Zarand calc-alkaline to

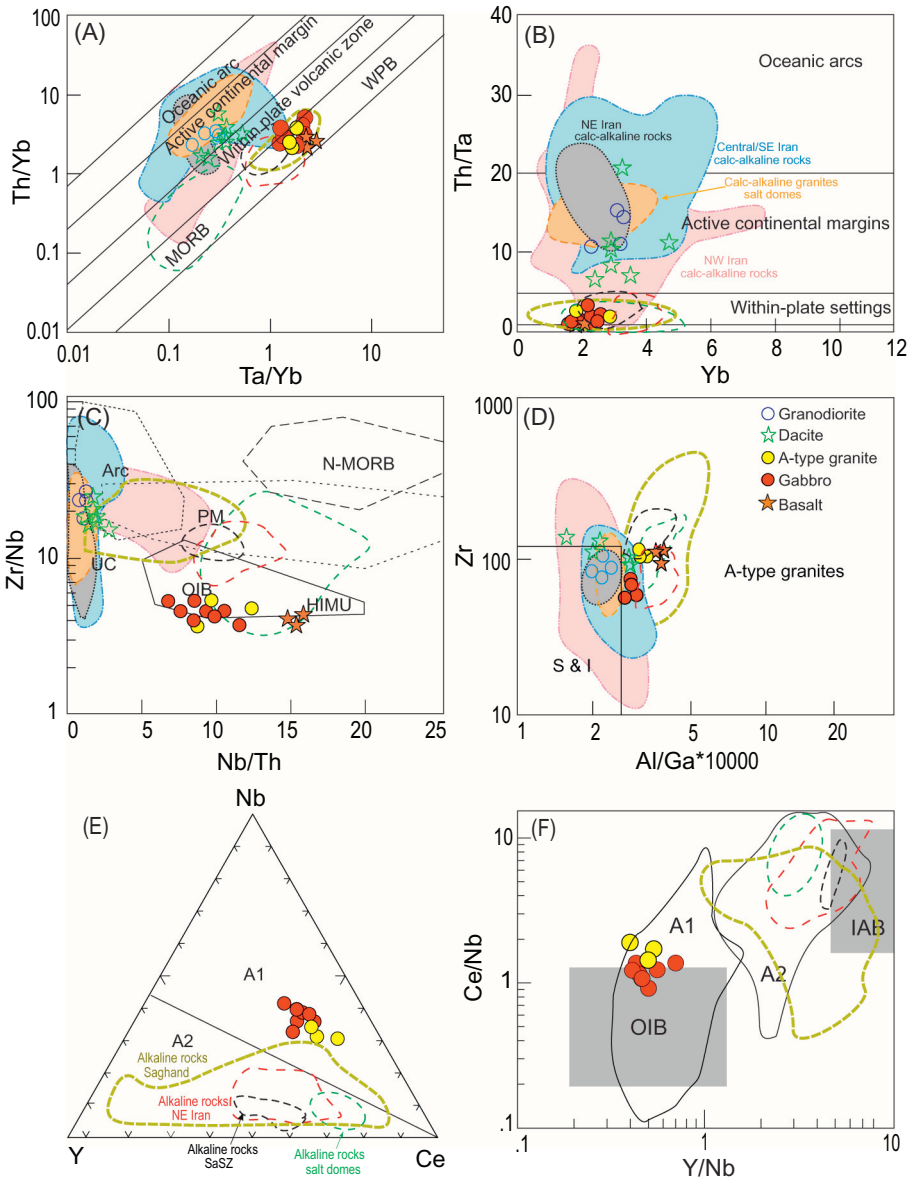

Fig. 8. Tectonic discrimination diagrams of Zarand Cadomian magmatic rocks. (A) Th/Yb *vs* Ta/Yb (Tindle and Pearce, 1983); (B) Th/Ta *vs* Yb (Schandl and Gorton, 2002); (C) Zr/Nb *vs* Nb/Th (Condie, 2005a) and (D) The Al/Ga*1000 *vs* Zr diagram (after (Whalen et al., 1987)). (E) Triangular Nb-Y-Ce and (F) Binary Ce/Nb *vs* Y/Nb diagrams (Eby, 1992b) for the classification of Zarand A-type granites. We also plotted OIB-gabbros for comparison, as these plots are based on the elemental ratio of immobile elements which can help us to understand compositional similarities between OIB-like mafic rocks and A-type granites. Data for Iran Cadomian rocks are from (Badr et al., 2013; Balaghi et al., 2014; Moghadam et al., 2015; Moghadam et al., 2016; Moghadam et al., 2017a). Bulk rock data for Cadomian exotic blocks within salt domes is from Asadi et al., (unpublished data). Data for NE and Central Iran alkaline mafic rocks are from (Balaghi et al., 2010; Maleki et al., 2019; Veiskarami et al., 2019), whereas data for Cadomian A_2-type granites from Sanandaj-Sirjan Zone are from (Shabanian et al., 2018; Shakerardakani et al., 2015). Data for Saghand rocks are from (Ramezani and Tucker, 2003).

shoshonitic felsic samples show high SiO_2 contents (68-72 *wt%*), low MgO (0.55-1.95 *wt%*) and non-radiogenic Nd isotope ($\varepsilon Nd(t) = -7.7$ to -6.2), suggesting they did not equilibrate with the upper mantle. This criterion, and the lack of the mafic counterparts in the study area, argues against derivation of the Zarand calc-alkaline to shoshonitic felsic magmas from mantle melts via FC. Generally, the felsic rocks of the Zarand rocks have high concentrations of Zr, Hf, LILEs and LREEs, typical of continental-arc magmas. Although these geochemical characteristics imply a crustal contribution, the depletion of Nb and other HFSEs relative to the LREEs, and enrichment of LILEs may be related to fluid-melt released from a down-going slab and mantle wedge melting or inherited from anatexis of a continental crust above a subduction regime.

Understanding the role of mafic continental lower crust in the genesis of high-K calc-alkaline to shoshonitic Zarand igneous rocks is challenging, because it is difficult to discriminate between fractionated mantle-derived melt and melts derived from partial melting of the juvenile lower crust. The non-radiogenic bulk $\varepsilon Nd(t)$ (-7.7 to -6.2) and zircon $\varepsilon Hf(t)$ (mean$= +1.6$) isotopic values for high-K calc-alkaline to shoshonitic Zarand igneous rocks does not favor melting of mafic continental lower crust, which is expected to be radiogenic. These felsic magmas may have formed by partial melting of older continental crust and/or via interaction of mantle melts with such crust via assimilation-fractional crystallization. Mixing of mantle-derived magmas with crustal melts is an alternative explanation. The peraluminous signature of these rocks confirm a crustal component in the genesis of these magmas, probably via crustal melting and fractional crystallization (Rudnick, 1992, 1995). Zarand high-K calc-alkaline-shoshonitic rocks have high concentrations of Th (high Th/Yb ratios of 1.7-6.3) with negative $\varepsilon Nd(t) = -6.2$ to -7.7), showing significant

influences of crustal components during magma genesis and evolution. Pb isotopes also attest to the involvement of crustal materials during the genesis of Zarand high-K calc-alkaline-shoshonitic rocks. The variable range of Hf isotopic composition of the zircons ($\varepsilon Hf(t) = -6.6$ to $+6.3$) rules out a simple evolution of the Zarand high-K calc-alkaline-shoshonitic melts by fractional crystallization, nevertheless other mechanisms such as wall-rock assimilation can explain the observed Hf isotope variations. Therefore, the heterogeneous distribution of the zircon Hf-isotope data, as well the whole-rock Nd isotopic compositions of Zarand high-K calc-alkaline-shoshonitic rocks show that mantle-derived magmas and pre-existing crustal material were involved in their genesis. The presence of xenocrystic zircons (with ages of 1.1 to 2.3 Ga) in Zarand high-K calc-alkaline-shoshonitic rocks further supports assimilation of older crust (Belousova et al., 2006; Griffin et al., 2002; Yang et al., 2008).

Although the role of crustal components during the genesis of Zarand high-K calc-alkaline-shoshonitic rocks is clear, it is difficult to simulate the composition of the precursor mantle melts that interacted with the continental crust to generate these magmas. In addition, it is challenging to unravel whether the high contents of K, Th and other incompatible elements come from melting of continental crust or these elements were supplied from melting of a metasomatized mantle wedge. Therefore, we suggest that melting of a metasomatized mantle wedge could be the source of mafic melt precursors to granitic magmatism in the Zarand region. In this scenario, underplating of the lower crust by mafic magmas led to partial melting of the lower crust, then assimilation-fractional crystallization generated granite melts (e.g., (Ferre and Leake, 2001; Karsli et al., 2010)). Furthermore, negative Eu anomalies indicates that these melts likely experienced low-pressure plagioclase fractionation in crustal magma chambers. Nd-isotope crustal residence ages (T_{DM}) of Zarand high-K calc-alkaline-shoshonitic rocks range from 1.5 to 1.6 Ga, suggesting that Mesoproterozoic or older crust was involved in their genesis. Moreover, zircon Hf T^{C}_{DM} ages are also a good indicator of the age of the older crust that contributed to the Cadomian magmas. Zarand zircon Hf TDM^{C}_{DM} model ages range between 0.9 and 1.9 Ga for calc-alkaline-shoshonitic rocks; except for one point with a model age of 3.4 Ga (Table S3). This inference also agrees with U-Pb ages of 1.1 to 2.3 Ga for inherited zircons separated from these rocks. In addition, compiled data from all of Iran show a prevalence of Hf model ages in the range of 1-3.7 Ga (Moghadam et al., 2017c). This is in agreement with the ages of inherited zircon cores from other Cadomian rocks which show dominant distribution at >600–1000 Ma and 2.4–2.5 to 3.6 Ga, which is consistent either with an original Cryogenian-Tonian to Archean crust with Gondwanan affinities (Honarmand et al., 2018b; Nutman et al., 2014; Shafaii Moghadam et al., 2020). From all this evidence, we infer that Zarand high-K calc-alkaline-shoshonitic rocks are the products of assimilation-fractional crystallization of originally mafic magmas derived from a metasomatized mantle wedge interacting with Proterozoic to Archean continental crust. Mixing between mafic magmas and secondary melts from Proterozoic to Archean continental crust is also possible. These secondary melts were generated by underplating of mafic magmas beneath the cratonic, old crust above the Cadomian subduction zone, which caused crustal anatexis.

5.2. Petrogenesis of Cadomian alkaline rocks

Zarand alkaline igneous rocks including granites, gabbros and basalts have similar ages to the high-K calcalkaline and shoshonitic suite. Granites have high contents of Na_2O, K_2O, FeO/MgO, Ga/Al and HFSEs, and low contents of CaO, Al_2O_3, Sc, Cr, Co and Ni. These rocks show enrichment in LREEs, Rb, Th, U, Pb and K, without depletion in Nb and Ti, in agreement with geochemical features of A-type magmas formed in continental rift zones (e.g., (Collins et al., 2019; Eby, 1990; Frost et al., 2002; Whalen et al., 1987). Zarand alkaline rocks plot in within-plate field in the Th/Yb *vs* Ta/Yb, Th/Ta *vs* Yb and Zr/Nb *vs* Nb/Th diagrams (Figs. 8A-C). Th/Ta ratios of the alkaline rocks range from 0.85 to 2.27, significantly lower than those of high-K calc-alkaline-shoshonitic rocks. In the Al/Ga×1000 *vs* Zr diagram (Fig. 8D), gabbros and granites are similar to within-plate A-type granites. The alkaline rocks are characterized by high concentrations of Yb (lower Th/Yb ratios of 1.8-3.8 compared to Zarand calc-alkaline-shoshonitic rocks) and positive εNd (t) values ($+0.3$ to $+4.0$), clearly showing more juvenile mantle-derived component than do high-K calc-alkaline-shoshonitic rocks.

On the triangular Nb-Y-Ce and the binary Ce/Nb *vs* Y/Nb diagrams (Eby, 1992b), the Zarand alkaline granites and gabbros plot in the A_1-type granite field (Figs. 8E-F). A-type granites and gabbros are also similar to OIB rocks in a Ce/Nb *vs* Y/Nb plot. This geochemical signatures for Zarand alkaline gabbros and A-type granites are different than Cadomian alkaline rocks from NE Iran, Sanandaj-Sirjan Zone and from the exotic blocks within the Cadomian salt domes, which are similar to A_2-type granites (Fig. 8E-F).

Several models have been proposed to explain the source and origin of A-type granites and their associated alkaline mafic rocks including: (1) Fractionation of a mantle-derived mafic alkaline magma to yield alkali-rich differentiates (Bonin, 2007); (2) Late stage alkali-, F- or Cl-rich solutions interact either with residual magmas- or metasomatically with pre-existing granites to generate A-type granites (Harris et al., 1986); (3) Melting of high grade felsic metamorphic rocks from which a previous melt phase had been extracted (Clemens, 1990). A_1-granites are peralkaline and thought to originate from differentiation of OIB-like magmas whereas A_2-granites are peraluminous and are interpreted as differentiation products of tholeiitic magmas and/or are the partial melting products of lower continental crust (Karsli et al., 2012; Karsli et al., 2018; Vasyukova and Williams-Jones, 2019). Therefore, the genesis of A_2-type granites needs crustal melting under high-T anhydrous conditions (Clemens, 1990; Clemens et al., 1986; Patiño Douce, 1997; Patiño Douce, 1999), which is consistent with their geochemical signatures (Eby, 1992a). Instead, the occurrence of A_1-type granites like those of Zarand can be related to fractionation of parental alkaline magma which was generated by decompression melting during lithospheric extension but without the influence of the advecting aqueous fluids from hydrous arc magmas. Zarand A_1-type granites are similar to alkaline gabbros in term of their Ce/Nb, Y/Nb, Zr/Nb, Nb-Y-Ce and Nd isotopic composition. Therefore, we propose that fractional crystallization of alkaline gabbros generated Zarand Cadomian A_1-type granites.

The mantle source of gabbros and basalts can be traced by their radiogenic $(^{143}Nd/^{144}Nd)_i$ isotopic ratios, HFSE concentrations and N-MORB-normalized patterns, which are similar to those of OIBs (Fig. 6), although they have more LILE content. Their high HFSE concentrations suggest generation of these alkaline rocks from an enriched mantle source. Enriched mantle sources such as EM-I and EM-II reservoirs may form alkaline magmas with negative $\varepsilon Nd(t)$ values (Zindler and Hart, 1986), in contrast to the $\varepsilon Nd(t)$ values of Zarand gabbros and basalts rocks which are positive. From this, we propose that Zarand basalts and gabbros were not formed from a long-lived enriched mantle sources (EM-I or EM-II) or involvement of crust components in their mantle reservoir. The range of $\varepsilon Nd(t)$ in basalts and gabbros, from $+0.3$ to $+4.0$, along with their enrichment in K, Rb, REEs and other HFSEs suggest a metasomatized mantle source such as SCLM- or OIB-like reservoir for their formation. There is no evidence for subduction components in the Zarand alkaline suite magmas and these are most consistent with formation in a continental rift.

5.3. Implications for Cadomian magmatism in Iran-Anatolia

One of the main inquiries related to the origin and evolution of the Cadomian Zarand magmatic rocks is how can we relate these to other exposures of similar age magmatic rocks elsewhere in Iran and Anatolia? Cadomian igneous rocks in Iran and Anatolia are mainly felsic intrusive rocks with less felsic extrusive rocks and are mostly geochemically

classified as Volcanic Arc Granites (VAG) (Moghadam et al., 2015; Moghadam et al., 2017a; Ustaomer et al., 2009).

Cadomian exposures in SE Anatolia are mainly metagranitoids and granitic to dioritic gneisses with zircon U-Pb ages of 572 to 529 Ma, which are hosted by Late Neoproterozoic schist, amphibolite and orthogeneiss. Volcanic rocks show zircon U-Pb ages of 581.4 ± 3.5 Ma and 559.2 ± 3.2 Ma for andesites and 569.6 ± 1.6 Ma, 571.6 ± 1.9 Ma and 575.4 ± 4.3 Ma for rhyolites (Beyarslan et al., 2016). Metagranitoids and granitic to dioritic gneisses are characterized by negative zircon εNd (t) values of −5.1 to −4.1 (Fig. 7B), whereas andesites and rhyolites have positive εNd(t) values of +0.5 to +4.2 (Fig. 7B) with low εHf (t) values of +0.4 to −5.3. These isotopic characteristics imply that Cadomian magmas from SE Anatolia experienced strong interaction with older continental crust (Ustaomer et al., 2009; Ustaomer et al., 2012). The Nd model ages suggest that Proterozoic crust of 1.1-2.1 Ga was involved in the genesis of these magmas.

Cadomian basement exposures are also found in NW Iran (*ca* 590-540 Ma (Honarmand et al., 2018b)), central Iran (*ca* 599-525 Ma (Ramezani and Tucker, 2003)), NE Iran (*ca* 560-525 Ma) and in the Sanandaj-Sirjan zone (*ca* 596-540 Ma (Hassanzadeh et al., 2008)). Cadomian exposures from NW Iran (Zanjan-Takan and Khoy-Salmas) are mostly composed of granitic to tonalitic gneisses, granitoids, migmatites, granulites along with rhyolites with zircon U-Pb ages of 620 to 500 Ma (Hassanzadeh et al., 2008; Moghadam et al., 2017a; Moghadam et al., 2017c; Moghadam et al., 2019). The magmatic rocks are characterized by low εHf(t) values of −7 to −0.7, suggesting significant involvement of older Proterozoic continental crust (1.1-2.3 Ga). However, some zircons have Archean Hf model ages (~2.5 Ga), suggesting the involvement of Archean crust. Archean detrital zircons are also widespread in Ediacaran to middle Paleozoic sedimentary rocks and may be derived from Gondwana or are inherited from hidden pre-Cadomian crust in Iran (Fergusson et al., 2016; Moghadam et al., 2017d; Nutman et al., 2014; Shakerardakani et al., 2019). Cadomian exposures from NW Iran also contain metamorphosed sandstones, metagraywackes and metapelites in association with tectonic slices and blocks of serpentinites and metaperidotites (Hajialioghli et al., 2007; Saki et al., 2011), which may be fragments of a Cadomian accretionary prism.

Cadomian rocks from NE Iran are mostly high-K calc-alkaline granitoids, gabbros to diorites, rhyolites and tuffs with zircon U-Pb ages of 530 to 556 Ma (Bagherzadeh et al., 2015; Moghadam et al., 2017c). Minor alkaline mafic rocks with zircon U-Pb ages of 545 to 555 Ma are also reported from NE Iran. The NE Iran high-K calc-alkaline magmatic rocks are characterized by εNd(t) values of −4 to +8.4 and εHf(t) of −3.4 to+8.5 (Bagherzadeh et al., 2015; Moghadam et al., 2017c), which is broadly similar to other Cadomian rocks from SE Anatolia and NW

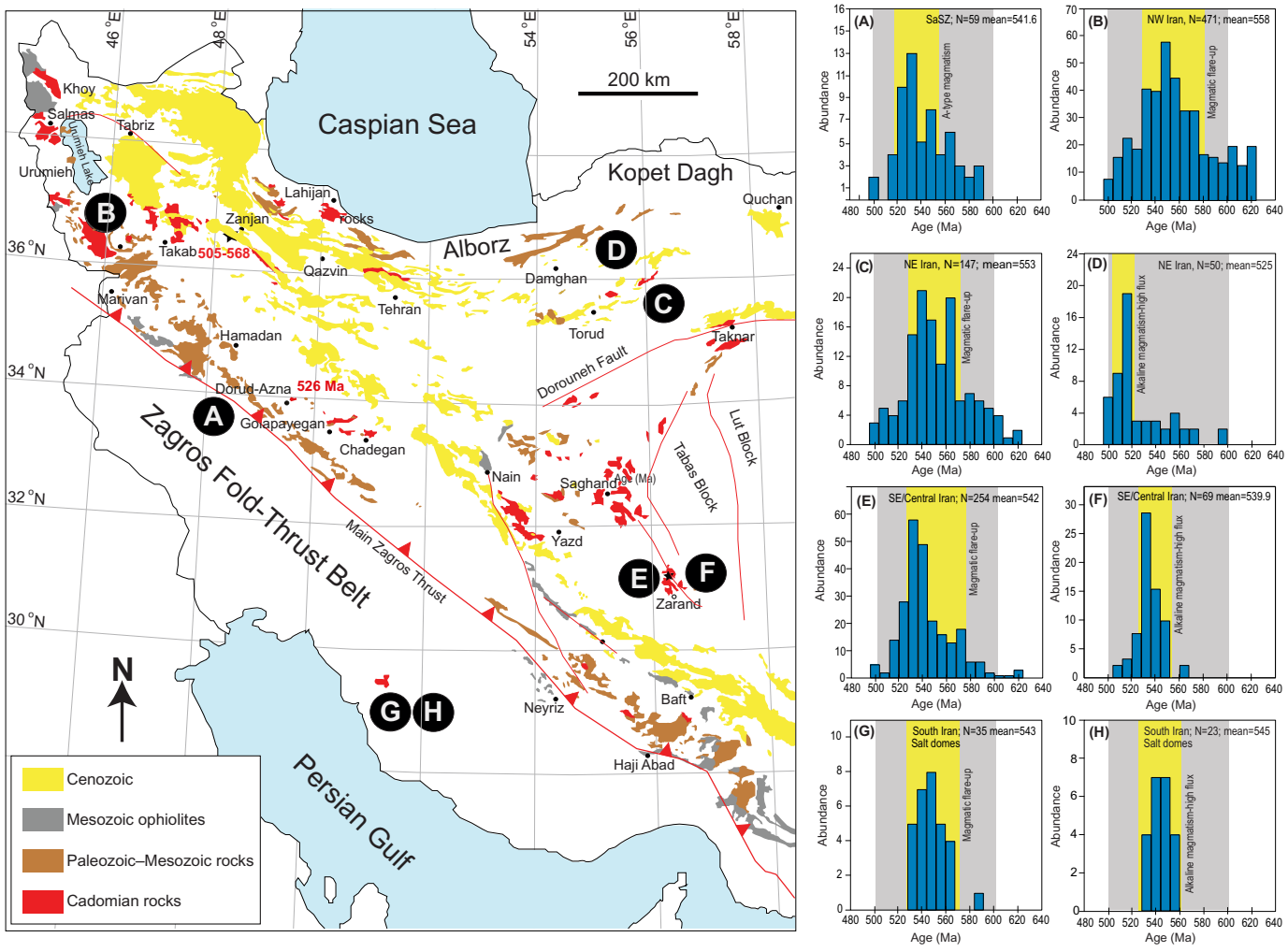

Fig. 9. Histograms showing the magmatic zircon age distribution of Cadomian rocks from Iran and Anatolia. Data for Iran and Turkey zircons are from (Badr et al., 2013; Balaghi et al., 2014; Gursu et al., 2015; Moghadam et al., 2015; Moghadam et al., 2016; Moghadam et al., 2017a; Ustaomer et al., 2009). Zircon U-Pb data for Cadomian exotic blocks within salt domes from S Iran is from Asadi et al., (unpublished data). Zircon data for NE and Central Iran rocks are from (Balaghi et al., 2010; Maleki et al., 2019; Veiskarami et al., 2019), whereas data for central Iran rocks are from (Ramezani and Tucker, 2003). Zircon U-Pb data for Cadomian A_2-type granites of the Sanandaj-Sirjan Zone come from (Shabanian et al., 2018; Shakerardakani et al., 2015).

Iran, which also show variable interaction with older continental crust. Alkaline mafic rocks from NE Iran are characterized by a stronger mantle signature (high Nb/Yb ratio, without Nb-Ta depletion). The generation of these alkaline magmas is attributed to an enriched mantle source (Balaghi et al., 2010; Veiskarami et al., 2019). Calc-alkaline and alkaline Cadomian xenoliths with similar ages (~538-540 Ma) are also reported from Saghand and salt domes of S Iran. Alkaline intrusive rock xenoliths from salt domes of S Iran are characterized by strong mantle signatures and positive initial εNd(t) values of +4.7 to +6.8 (Asadi et al., unpublished data).

In summary, the heterogeneous distribution of zircon Hf-isotope data as well as whole-rock Nd isotopic compositions of Cadomian calc-alkaline rocks with subduction signatures from Iran and Anatolia indicate that two discrete components - mantle-derived magmas and pre-existing continental crust or sediments - were involved in their genesis. The role of pre-existing continental crust component may decrease from SE (Zarand) toward NE and NW Iran.

Cadomian rocks from Zarand are geochemically bimodal and include both high-K calc-alkaline-shoshonitic rocks and alkaline rocks. Alkaline rocks have no Nb-Ta anomalies with radiogenic Pb isotopic composition. Cadomian alkaline rocks (OIB-like mafic rocks and A-type granites) have rarely reported from other Cadomian exposures of Iran, such as those from NE, Central and S Iran as well as the Sanandaj-Sirjan Zone. Part of this rarity seems to be related to the paucity of geochemical data from the Cadomian exposures of Iran. Our new data indicate that Zarand alkaline rocks are characterized by a stronger mantle signature, with εNd(t) and εHf(t) values of +0.3 to +4.0 and +1.1 to +5.1, respectively. The generation of these alkaline magmas requires the involvement of somewhat enriched mantle.

Cadomian magmatic rocks in Iran and Anatolia are suggested to have formed during a magmatic flare-up that lasted ~44 Myr, from ~572 Ma until 528 Ma (Moghadam et al., 2017e). Our new and compiled data (Fig. 9) are consistent with this general assessment but also show the high-flux magmatism- within this interval- occurred at various times in different parts of Iran. For example, in central/SE and NW Iran, the flare-up lasted from ~580 to 530 Ma, while magmatism started by ~620 Ma. Alkaline magmatism in central/SE Iran seems to have waned earlier, at ~550 Ma. In NE Iran magmatic flare-up lasted for ~40 Myr from 570 to 530 Ma and alkaline magmatism mainly lasted ~20 Ma (520-500 Ma). In contrast, magmatic flare-up in S Iran and Sanandaj-Sirjan Zone happened at 570 to 530 Ma and 550-520 Ma, respectively (Fig. 9).

5.4. Geodynamic implications for the formation of Zarand Cadomian igneous rocks

Zarand Ediacaran-Early Paleozoic sedimentary and magmatic rocks are broadly similar to rocks from other Cadomian exposures in Iran and Anatolia. However, there are differences in inferred magmato-depositional environments relative to the likely trend and location of the main magmatic arc, which lay to the north. Most Cadomian magmatic rocks in Iran-Anatolia formed as parts of the magmatic arc.

The most important new result of our studies is the discovery of Cadomian alkaline rocks in the Zarand region. These alkaline rocks are geochronologically similar to calc-alkaline rocks, with both forming at ~535 Ma. In support of geochemical and isotopic evidence for a rift basin origin for the alkaline rocks, there is a relationship between the presence of the alkaline suite and sediment thickness. Thick sequences of terrigenous rocks with minor evaporites in Rizu-Dezo Formation, similar to the Hormoz series to the south, support deposition in a rift basin. The deposition of banded iron-salt deposits- mainly in the Hormoz series- at about this time also indicate deposition in a rift basin (Atapour and Aftabi, 2017a; Atapour and Aftabi, 2017b).

Alkaline magmatic rocks are rare among the Cadomian terranes of Iran and Anatolia but are reported from Central (e.g., (Ramezani and Tucker, 2003)) and NW Iran (e.g., (Hassanzadeh et al., 2008)) where they occur as rhyolitic flows. Igneous rocks with alkaline signatures are also present as Cadomian exotic blocks within the salt domes of S Iran (Faramarzi et al., 2015). The mafic alkaline rocks and their metamorphosed (lower amphibolite facies) equivalents are also reported from Central and NE Iran (Balaghi et al., 2010; Maleki et al., 2019; Veiskarami et al., 2019). In addition, Cadomian A_2-type granites have been reported from the Sanandaj-Sirjan Zone of Iran (Shabanian et al., 2018; Shakerardakani et al., 2015). Alkaline rhyolites are also reported from Saghand (Momenzadeh and Heidari, 1995). Higher alkalies and incompatible elements in these rhyolites show their highly fractionated nature; these are not really alkaline volcanic rocks. These rocks are suggested to have formed in a subduction-related setting (Ramezani and Tucker, 2003), in contrast to a rift-environment proposed by others (Momenzadeh and Heidari, 1995).

All studied Cadomian exposures from Iran, Anatolia, Taurids and Iberia comprise both magmatic and sedimentary rocks (and/or their metamorphic equivalents, metamorphosed in greenschist to amphibolite facies) with minor high-pressure metamorphic rocks (eclogites) and Cadomian ophiolites (Moghadam et al., 2017a; Moghadam et al., 2017b). The ratio of magmatic to sedimentary rocks varies from exposure to exposure. The presence of ophiolite and high-pressure rocks shows the presence of a fossilized subduction-related forearc and accretionary prism. Such ophiolites and high-P rocks are present in Iberia and Taurides (Candan et al., 2015; Kounov et al., 2012). The extensive occurrence of plutonic to volcanic calc-alkaline rocks (both spatially and compared to alkaline rocks) in Cadomian exposures probably show a main arc (magmatic front). These exposures usually contain minor volcanic rocks which probably eroded extensively during Ediacaran-early Paleozoic and/or younger tectonic processes. The assumed magmatic front contains minor sediments, most of which are metamorphosed into greenschists and paragneiss. These rocks contain prevalent 600-500 Ma old detrital zircons (~70-90%), with minor (30-10%) older zircons (Balaghi et al., 2014). In contrast, suspected retro-arc exposures such as Zarand contain minor plutonic rocks, with subordinate volcanic rocks interlayered with terrigenous sedimentary rocks (Fig. 10). Therefore, the volume of magmatism in the Iran Cadomian retro-arc was less than at the magmatic front to the north. These sedimentary rocks (which mostly are non-metamorphosed) contain abundant Archean and Paleoproterozoic as well as Cadomian zircons, which show strong crustal reworking and a supply from a both juvenile crust of Arabia and cratonic crust of Africa (Drost et al., 2004; Drost et al., 2011; Linnemann et al., 2011; Moghadam et al., 2017b; Pereira et al., 2006; Pereira et al., 2012). These sediments were supplied from these regions via super-fan systems or detrital sheets (Meinhold et al., 2013) (Fig. 10). Archean and Paleoproterozoic xenocrystic zircons and/or zircon cores are also present in metasedimentary rocks (e.g., paragneisses) from other Cadomian terranes (e.g., from NW Iran), but the ratio of Cadomian to Archean -Paleoproterozoic zircons are much higher than found in Zarand retro-arc sediments.

In summary, although there are two types of igneous rocks in the Zarand region, the calc-alkaline-shoshonitic and alkaline suites formed simultaneously in a single tectonic setting (Fig. 10). The presence of alkaline rocks is important for showing the location of a continental rift behind the continental arc, as is seen elsewhere (e.g., Iran Paleogene arcs, (Moghadam et al., 2018; Sepidbar et al., 2019)). Such extensional rifts can be related to slab roll-back which can also be responsible for arc magmatic flare-ups and exhumation of subduction-related high-pressure rocks (Ducea et al., 2017). Slab rollback may have been especially important because this causes extension, crustal thinning, continental rifting and juvenile crustal addition (Miskovic and Schaltegger, 2009). Extension and crustal thinning permit decompression melting of the subcontinental lithospheric mantle (=SCLM) or sub-arc mantle beneath the retro-arc (Fig. 10B). Low degree of melting of an enriched SCLM and/or plume-influenced sub-arc mantle can generate OIB-like melts. Such melts may differ from OIB-like melts from oceanic Islands and/or continental plumes which are more undersaturated and

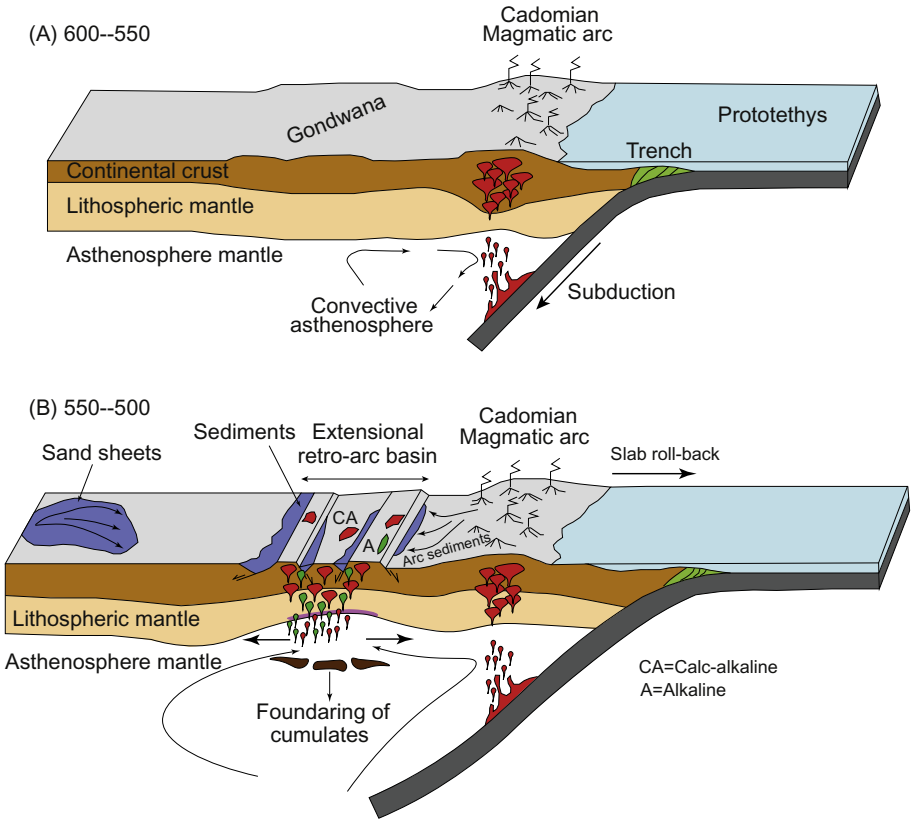

Fig. 10. Summary of the tectonic evolution of Cadomian (600-500 Ma) rocks from SE Iran (and North Gondwana) (see text for explanations).

isotopically evolved. Plumes also affect a larger area, with a diameter of ~>300 km (e.g., (Poore et al., 2011)), which is not the case for Iran's Cadomian terranes. Fractionation of primary OIB-like melts can produce gabbros and then upon more fractionation to crystallize A_1-type granites. These mantle melts can also provide heat to melt continental crust to produce Zarand calc-alkaline-shoshonitic rocks via assimilation and fractional crystallization. However, we cannot rule out the effect of flux melting in the sub-arc mantle beneath the retro-arc basin which can also generate mafic melts that can interact with overlying continental crust to produce Zarand calc-alkaline-shoshonitic rocks via assimilation and fractional crystallization. Retro-arc calc-alkaline rocks- such as Zarand rhyolites-dacites and granodiorites- are geochemically similar to Cadomian calc-alkaline rocks from the magmatic front (Figs. 5, 7-8), although retro-arc calc-alkaline rocks show more negative εNd(t) values and higher Pb isotopic compositions along with higher Rb, K and A/CNK ratios.

Another alternative for the generation of Zarand OIB-like mafic rocks is low-degree melting of asthenospheric mantle accompanying delamination. Influx of asthenospheric materials to the arc root, due to the foundering of dense cumulates, may trigger the generation of more mafic magmas. This process has been suggested to explain the isotopic disruption of magmatic rocks from other arcs (e.g., (Paterson and Ducea, 2015; Stuart et al., 2016)). Foundering of Cadomian arc cumulates is evidenced by the presence of garnet-amphibole bearing ultramafic-mafic cumulates from NE Iran (Shafaii Moghadam et al., 2020) (Fig. 10B). Cadomian alkaline magmatism started at ~550 Ma, which accords well with zircon U-Pb ages of the foundered cumulates. Considering upwelling rate of asthenosphere instabilities of ~270 mm/yr. (Poore et al., 2011), a maximum upwelling of ~13.5 meter is expected for the asthenosphere materials during 50 m.yr. (550-500 Ma), depending on mantle temperature and extensional regimes in the overlying plate. This may explain why alkaline rocks are rare even in the retro-arc setting of Cadomian arcs. It seems that Cadomain magmatism- with strong subduction signatures- continued in the main arc until ~500 Ma, whereas magmatism in retro-arc probably died earlier.

6. Conclusions

1- Cadomian magmatic high K calc-alkaline -shoshonitic to alkaline rocks from Zarand (SE Iran) were formed during southward subduction of Prototethyan oceanic lithosphere accompanied by Late Neoprotozoic-Early Cambrian back-arc extension in a continental arc setting. Zircon U-Pb geochronology indicate that the high K calc-alkaline -shoshonitic rocks and A-type granites from Zarand have almost identical ages of 537-536 and 535 Ma, respectively.

2- Trace element geochemistry, bulk-rock Nd and zircon Hf-isotope composition indicate involvement of both juvenile melts and an older continental crust during the generation of high K calc-alkaline-shoshonitic rock, whereas an enriched mantle was responsible for the genesis of alkaline rocks.

3- At *ca* 590-560 Ma, a back-arc/rifted retro-arc basin formed behind the Cadomian magmatic arc. The formation of this basin was caused by crustal stretching due to the subduction of Prototethyan ocean beneath N Gondwana. The retro-arc basin was filled by detrital sediments of eroded Cadomian arcs and by juvenile and reworked old components of both Arabian plate and African craton of Gondwana.

Supplementary data to this article can be found online at https://doi.org/10.1016/j.lithos.2020.105569.

Declaration of Competing Interest

The authors declare that they have no known competing financial interests or personal relationships that could have appeared to influence the work reported in this paper.

Acknowledgments

AcknowledgmentsWe are very grateful to Gültekin Topuz and an anonymous reviewer for their constructive reviews of the manuscript. Editorial suggestions by Xian-Hua Li are appreciated. This is UTD Geosciences Dept. contribution # 1365. F. Sepidbar acknowledges support from the Iran Science Elites Federation. F.S. also thanks university of Damghan for assistance during the field work.

Appendix A

Zircon grains from four rock samples were separated using conventional magneto separator and heavy liquid techniques. Subsequently, representative zircon grains were handpicked, mounted in epoxy resin, polished and coated with a film for CL imaging. All grains were imaged by CL and BSE to provide maps to guide the choice of analytical spots. Zircon U-Pb dating analysis was performed at Key Laboratory of Mineralogy and Metallogeny, Guangzhou Institute of Geochemistry, Chinese Academy of Sciences, Guangzhou (China) by Laser ablation multi-collector inductively coupled plasma mass spectrometry (LA-MC-ICPMS). Laser ablation was performed using a RESOlutin M-50 system equipped with a 193 nm ArF-excimer laser. A Neptune Plus MC853 was used to acquire ion-signal intensities. Detailed descriptions of both instruments were reported in (Zhang et al., 2014). The laser beam has a diameter of 24 μm, a repetition frequency of 6 Hz and energy density of ~5 J cm^{-2}. Five ion counters were used to detect the signals of ^{202}Hg, ^{204}Pb, ^{206}Pb, ^{207}Pb and ^{208}Pb. ^{232}Th and ^{238}U were collected by Faraday cups. Zircon 91500 was used as the external standard for U-Pb dating. Preferred U-Th-Pb isotope ratios used for zircon 91500 are from (Wiedenbeck et al., 1995). Uncertainty of preferred values for the standard 91500 was propagated to the final results of the samples. Zircon standard Plešovice (Slama et al., 2008) was analyzed as an unknown. U-Pb isotopic ages were calculated using the ISOPLOT program of (Ludwig, 2003). Zircon U-Pb ages are presented in Table S1. Major element composition of samples was analyzed at the State Key Laboratory of Ore Deposit Geochemistry, Institute of Geochemistry, Chinese Academy of Sciences, Guizhou (China). The precision of analysis, based on the repeated analyses, is ±1.0% for major elements, whereas most trace elements have an uncertainty of ±5.0%. Whole-rock major- and trace-elements data are presented in Table S2. In-situ zircon Hf isotopic analyses were obtained using LA-MC-ICPMS at Key Laboratory of Mineralogy and Metallogeny, Guangzhou Institute of Geochemistry, Chinese Academy of Sciences, Guangzhou (China). During the analysis, a laser repetition rate of 7 Hz was used with the spot size of 45 μm. Each spot analysis consists of 20 s gas blank collection with laser off and 30s sample signal collection with laser on. All isotope signals were detected with Faraday cups. The isobaric interferences of ^{176}Yb and ^{176}Lu on 176Hf were corrected with the signal intensities of 173Yb and ^{175}Lu combined with the natural ratios of $^{176}Yb/^{173}Yb$ and $^{176}Lu/^{175}Lu$. The $^{176}Hf/^{177}Hf$ was normalized to $^{179}Hf/^{177}Hf$ of 0.7325 using an exponential law for mass bias correction. During the analysis, the $^{176}Hf/^{177}Hf$ ratio of the standard zircon (Penglai) was 0.282915 ± 0.000022 (2σ), agreeing with the recommended values within 2σ error (Li et al., 2010). Zircon Hf isotope data are presented in Table S3.

Sr and Nd isotope ratios were determined at Key Laboratory of Mineralogy and Metallogeny, Guangzhou Institute of Geochemistry, Chinese Academy of Sciences, Guangzhou (China). Samples for Sr-Nd isotopic analysis were dissolved in Teflon bombs by HF + HNO_3 mixture acid. Sr and Nd were separated using conventional ion exchange procedures and measured using a Neptune Plus MC-ICP-MS. Procedure blanks of the total chemical treatment was at the level of less than 1 ng for Nd and Sr. During the period of laboratory analysis, measurements of NIST SRM- Sr standard yielded $^{87}Sr/^{86}Sr$ ratio of 0.710250 ± 0.000030 (2σ), and the JNdi-1 Nd standard yielded $^{143}Nd/^{144}Nd$ ratio of 0.512115 ± 0.000004 (2σ). The detailed Sr-Nd analytical technique and correction procedure is provided in (Wu et al., 2006). The whole rock Sr-Nd isotope data are presented in Table S4.

References

Abbo, A., Avigad, D., Gerdes, A., Gungor, T., 2015. Cadomian basement and Paleozoic to Triassic siliciclastics of the Taurides (Karacahisar dome, south-central Turkey): Paleogeographic constraints from U-Pb-Hf in zircons. Lithos 227, 122–139.

Atapour, H., Aftabi, A., 2017a. Comments on "Geochronology and geochemistry of rhyolites from Hormuz Island, southern Iran: A new Cadomian arc magmatism in the Hormuz Formation". In: Faramarzi, N.S., Amini, S., Schmitt, A.K., Hassanzadeh, J., Borg, G., McKeegan, K., Razavi, S.M.H., Mortazavi, S.M. (Eds.), Lithos. 284, pp. 779–782 Sep. 2015, V.236-237, P.203-211: A missing link of Ediacaran A-type rhyolitic volcanism associated with glaciogenic banded iron salt formation (BISF). Lithos.

Atapour, H., Aftabi, A., 2017b. The possible synglaciogenic Ediacaran hematitic banded iron salt formation (BISF) at Hormuz Island, southern Iran: Implications for a new style of exhalative hydrothermal iron-salt system. Ore Geology Reviews 89, 70–95.

Avigad, D., Abbo, A., Gerdes, A., 2016. Origin of the Eastern Mediterranean: Neotethys rifting along a cryptic Cadomian suture with Afro-Arabia. Geological Society of America Bulletin 128, 1286–1296.

Badr, M.J., Collins, A.S., Masoudi, F., Cox, G., Mohajjel, M., 2013. The U-Pb age, geochemistry and tectonic significance of granitoids in the Soursat Complex, Northwest Iran. Turkish Journal of Earth Sciences 22, 1–31.

Bagherzadeh, R.M., Karimpour, M.H., Farmer, G.L., Stern, C.R., Santos, J.F., Rahimi, B., Heidarian Shahri, M.R., 2015. U–Pb zircon geochronology, petrochemical and Sr–Nd isotopic characteristic of Late Neoproterozoic granitoid of the Bornaward Complex (Bardaskan-NE Iran). Journal of Asian Earth Sciences 111, 54–71.

Baier, J., Audetat, A., Keppler, H., 2008. The origin of the negative niobium tantalum anomaly in subduction zone magmas. Earth and Planetary Science Letters 267, 290–300.

Balaghi, Z., Sadeghian, M., Ghasemi, H., 2010. Petrogenesis of the lower Paleozoic igneous rocks south of Bahabad (Bafq-Central Iran): Implication for rifting. Petrology 4, 45–64.

Balaghi, M.E., Mahmoud, S., Zhai, M.G., Habibollah, G., Mohammad, M., 2014. Zircon U-Pb ages, Hf isotopes and geochemistry of the schists, gneisses and granites in Delbar Metamorphic-Igneous Complex, SE of Shahrood (Iran): Implications for Neoproterozoic geodynamic evolutions of Central Iran. Journal of Asian Earth Sciences 92, 92–124.

Belousova, E., Griffin, W.L., O'Reilly, S.Y., Fisher, N., 2002. Igneous zircon: trace element composition as an indicator of source rock type. Contributions to Mineralogy and Petrology 143, 602–622.

Belousova, E.A., Griffin, W.L., O'Reilly, S.Y., 2006. Zircon crystal morphology, trace element signatures and Hf isotope composition as a tool for petrogenetic modelling: Examples from Eastern Australian granitoids. Journal of Petrology 47, 329–353.

Berberian, M., King, G.C.P., 1981. Towards a Paleogeography and Tectonic Evolution of Iran. Canadian Journal of Earth Sciences 18, 210–265.

Beyarslan, M., Lin, Y.C., Bingol, A.F., Chung, S.L., 2016. Zircon U-Pb age and geochemical constraints on the origin and tectonic implication of Cadomian (Ediacaran-Early Cambrian) magmatism in SE Turkey. Journal of Asian Earth Sciences 130, 223–238.

Bonin, B., 2007. A-type granites and related rocks: evolution of a concept, problems and prospects. Lithos 97, 1–29.

Candan, O., Koralay, O.E., Topuz, G., Oberhänsli, R., Fritz, H., Collins, A.S., Chen, F., 2015. Late Neoproterozoic gabbro emplacement followed by early Cambrian eclogite-facies metamorphism in the Menderes Massif (WTurkey). Implications on the final assembly of Gondwana. Research, Gondwana.

Clemens, J., 1990. The granulite—granite connexion, Granulites and crustal evolution. Springer, pp. 25–36.

Clemens, J., Holloway, J.R., White, A., 1986. Origin of an A-type granite; experimental constraints. American Mineralogist 71, 317–324.

Cocks, L.R.M., Torsvik, T.H., 2002. Earth geography from 500 to 400 million years ago: a faunal and palaeomagnetic review. Journal of the Geological Society 159, 631–644.

Collins, W.J., Huang, H.-Q., Bowden, P., Kemp, A.T.I., 2019. Repeated S-I-A-type granite trilogy in the Lachlan Orogen, and geochemical contrasts with A-type granites in Nigeria: Implications for petrogenesis and tectonic discrimination. Geological society, london, special publications 491 SP491-2018-2159.

Condie, K.C., 2005a. High field strength element ratios in Archean basalts: a window to evolving sources of mantle plumes? Lithos 79, 491–504.

Condie, K.C., 2005b. TTGs and adakites: are they both slab melts? Lithos 80, 33–44.

Crowley, Q.G., Floyd, P.A., Winchester, J.A., Franke, W., Holland, J.G., 2000. Early Palaeozoic rift-related magmatism in Variscan Europe: fragmentation of the Armorican Terrane Assemblage. Terra Nova 12, 171–180.

Defant, M., Jackson, T., Drummond, M., De Boer, J., Bellon, H., Feigenson, M., Maury, R., Stewart, R., 1992. The geochemistry of young volcanism throughout western Panama and southeastern Costa Rica: an overview. Journal of the Geological Society 149, 569–579.

Drost, K., Linnemann, U., McNaughton, N., Fatka, O., Kraft, P., Gehmlich, M., Tonk, C., Marek, J., 2004. New data on the Neoproterozoic - Cambrian geotectonic setting of the Tepla-Barrandian volcano-sedimentary successions: geochemistry, U-Pb zircon ages, and provenance (Bohemian Massif, Czech Republic). International Journal of Earth Sciences 93, 742–757.

Drost, K., Gerdes, A., Jeffries, T., Linnemann, U., Storey, C., 2011. Provenance of Neoproterozoic and early Paleozoic siliciclastic rocks of the Tepla-Barrandian unit (Bohemian Massif): Evidence from U-Pb detrital zircon ages. Gondwana Research 19, 213–231.

Ducea, M.N., Otamendi, J.E., Bergantz, G., Stair, K.M., Valencia, V.A., Gehrels, G.E., 2010. Timing constraints on building an intermediate plutonic arc crustal section: U- Pb

zircon geochronology of the Sierra Valle Fertil-La Huerta, Famatinian arc. Argentina. Tectonics 29.
Ducea, M.N., Bergantz, G.W., Crowley, J.L., Otamendi, J., 2017. Ultrafast magmatic buildup and diversification to produce continental crust during subduction. Geology 45, 235–238.
Eby, G.N., 1990. The A-type granitoids - a review of their occurrence and chemical characteristics and speculations on their petrogenesis. Lithos 26, 115–134.
Eby, G.N., 1992a. Chemical Subdivision of the a-Type Granitoids - Petrogenetic and Tectonic Implications. Geology 20, 641–644.
Eby, G.N., 1992b. Chemical subdivision of the A-type granitoids: petrogenetic and tectonic implications. Geology 20, 641–644.
Etemad-Saeed, N., Hosseini-Barzi, M., Adabi, M.H., Miller, N.R., Sadeghi, A., Houshmandzadeh, A., Stockli, D.F., 2015. Evidence for ca. 560Ma Ediacaran glaciation in the Kahar Formation, central Alborz Mountains, northern Iran. Gondwana Research.
Faramarzi, N.S., Amini, S., Schmitt, A.K., Hassanzadeh, J., Borg, G., McKeegan, K., Razavi, S.M.H., Mortazavi, S.M., 2015. Geochronology and geochemistry of rhyolites from Hormuz Island, southern Iran: A new record of Cadomian arc magmatism in the Hormuz Formation. Lithos 236, 203–211.
Fergusson, C.L., Nutman, A.P., Mohajjel, M., Bennett, V.C., 2016. The Sanandaj-Sirjan Zone in the Neo-Tethyan suture, western Iran: Zircon U-Pb evidence of late Palaeozoic rifting of northern Gondwana and mid-Jurassic orogenesis. Gondwana Research 40, 43–57.
Ferre, E.C., Leake, B.E., 2001. Geodynamic significance of early orogenic high-K crustal and mantle melts: example of the Corsica Batholith. Lithos 59, 47–67.
Frost, C.D., Frost, B.R., Bell, J.M., Chamberlain, K.R., 2002. The relationship between A-type granites and residual magmas from anorthosite: evidence from the northern Sherman batholith, Laramie Mountains, Wyoming, USA. Precambrian Research 119, 45–71.
Garfunkel, Z., 2015. The relations between Gondwana and the adjacent peripheral Cadomian domain—constrains on the origin, history, and paleogeography of the peripheral domain. Gondwana Research. 28, 1257–1281.
Griffin, W.L., Wang, X., Jackson, S.E., Pearson, N.J., O'Reilly, S.Y., Xu, X.S., Zhou, X.M., 2002. Zircon chemistry and magma mixing, SE China: In-situ analysis of Hf isotopes, Tonglu and Pingtan igneous complexes. Lithos 61, 237–269.
Gursu, S., Moller, A., Goncuoglu, M.C., Koksal, S., Demircan, H., Koksal, F.T., Kozlu, H., Sunal, G., 2015. Neoproterozoic continental arc volcanism at the northern edge of the Arabian Plate, SE Turkey. Precambrian Research 258, 208–233.
Hajialioghli, R., Moazzen, M., Droop, G.T.R., Oberhansli, R., Bousquet, R., Jahangiri, A., Ziemann, M., 2007. Serpentine polymorphs and P-T evolution of metaperidotites and serpentinites in the Takab area, NW Iran. Mineralogical Magazine 71, 203–222.
Harris, N.B., Pearce, J.A., Tindle, A.G., 1986. Geochemical characteristics of collision-zone magmatism. Geological society, london, special publications 19, 67–81.
Hassanzadeh, J., Stockli, D.F., Horton, B.K., Axen, G.J., Stockli, L.D., Grove, M., Schmitt, A.K., Walker, J.D., 2008. U-Pb zircon geochronology of late Neoproterozoic-Early Cambrian granitoids in Iran: Implications for paleogeography, magmatism, and exhumation history of Iranian basement. Tectonophysics 451, 71–96.
Hildreth, W., Halliday, A.N., Christiansen, R.L., 1991. Isotopic and Chemical Evidence Concerning the Genesis and Contamination of Basaltic and Rhyolitic Magma beneath the Yellowstone Plateau Volcanic Field. Journal of Petrology 32, 63–138.
Honarmand, M., Xiao, W., Nabatian, G., Blades, M.L., dos Santos, M.C., Collins, A.S., Ao, S., 2018a. Zircon U-Pb-Hf isotopes, bulk-rock geochemistry and Sr-Nd-Pb isotopes from late Neoproterozoic basement in the Mahneshan area, NW Iran: Implications for Ediacaran active continental margin along the northern Gondwana and constraints on the late Oligocene crustal anatexis. Gondwana Research 57, 48–76.
Honarmand, M., Xiao, W.J., Nabatian, G., Blades, M.L., dos Santos, M.C., Collins, A.S., Ao, S.J., 2018b. Zircon U-Pb-Hf isotopes, bulk-rock geochemistry and Sr-Nd-Pb isotopes from late Neoproterozoic basement in the Mahneshan area, NW Iran: Implications for Ediacaran active continental margin along the northern Gondwana and constraints on the late Oligocene crustal anatexis. Gondwana Research 57, 48–76.
Horton, B.K., Hassanzadeh, J., Stockli, D.F., Axen, G.J., Gillis, R.J., Guest, B., Amini, A., Fakllari, M.D., Zamanzadeh, S.M., Grove, M., 2008. Detrital zircon provenance of Neoproterozoic to Cenozoic deposits in Iran: Implications for chronostratigraphy and collisional tectonics. Tectonophysics 451, 97–122.
Hosseini, S.H., Sadeghian, M., Zhai, M.G., Ghasemi, H., 2015. Petrology, geochemistry and zircon U-Pb dating of Band-e-Hezarchah metabasites (NE Iran): An evidence for back-arc magmatism along the northern active margin of Gondwana. Chemie Der Erde-Geochemistry 75, 207–218.
Huang, H.Q., Li, X.H., Li, Z.X., Li, W.X., 2013. Intraplate crustal remelting as the genesis of Jurassic high-K granites in the coastal region of the Guangdong Province, SE China. Journal of Asian Earth Sciences 74, 280–302.
Karsli, O., Dokuz, A., Uysal, I., Aydin, F., Chen, B., Kandemir, R., Wijbrans, J., 2010. Relative contributions of crust and mantle to generation of Campanian high-K calc-alkaline I-type granitoids in a subduction setting, with special reference to the Harsit Pluton, Eastern Turkey. Contributions to Mineralogy and Petrology 160, 467–487.
Karsli, O., Dokuz, A., Uysal, İ., Ketenci, M., Chen, B., Kandemir, R., 2012. Deciphering the shoshonitic monzonites with I-type characteristic, the Sisdağı pluton, NE Turkey: magmatic response to continental lithospheric thinning. Journal of Asian Earth Sciences 51, 45–62.
Karsli, O., Aydin, F., Uysal, I., Dokuz, A., Kumral, M., Kandemir, R., Budakoglu, M., Ketenci, M., 2018. Latest Cretaceous "A(2)-type" granites in the Sakarya Zone, NE Turkey: Partial melting of mafic lower crust in response to roll-back of Neo-Tethyan oceanic lithosphere. Lithos 302, 312–328.
Kounov, A., Graf, J., von Quadt, A., Bernoulli, D., Burg, J.P., Seward, D., Ivanov, Z., Fanning, M., 2012. Evidence for a "Cadomian" ophiolite and magmatic-arc complex in SW Bulgaria. Precambrian Research 212, 275–295.
Kroner, A., Sengor, A.M.C., 1990. Archean and Proterozoic Ancestry in Late Precambrian to Early Paleozoic Crustal Elements of Southern Turkey as Revealed by Single-Zircon Dating. Geology 18, 1186–1190.
Lebas, M.J., Lemaitre, R.W., Streckeisen, A., Zanettin, B., 1986. A Chemical Classification of Volcanic-Rocks Based on the Total Alkali Silica Diagram. Journal of Petrology 27, 745–750.
Li, X.H., Long, W.G., Li, Q.L., Liu, Y., Zheng, Y.F., Yang, Y.H., Chamberlain, K.R., Wan, D.F., Guo, C.H., Wang, X.C., Tao, H., 2010. Penglai Zircon Megacrysts: A Potential New Working Reference Material for Microbeam Determination of Hf-O Isotopes and U-Pb Age. Geostandards and Geoanalytical Research 34, 117–134.
Li, J.H., Dong, S.W., Cawood, P.A., Zhao, G.C., Johnston, S.T., Zhang, Y.Q., Xin, Y.J., 2018. An Andean-type retro-arc foreland system beneath northwest South China revealed by SINOPROBE profiling. Earth and Planetary Science Letters 490, 170–179.
Linnemann, U., Pereira, F., Jeffries, T.E., Drost, K., Gerdes, A., 2008. The Cadomian Orogeny and the opening of the Rheic Ocean: The diacrony of geotectonic processes constrained by LA-ICP-MS U-Pb zircon dating (Ossa-Morena and Saxo-Thuringian Zones, Iberian and Bohemian Massifs). Tectonophysics 461, 21–43.
Linnemann, U., Ouzegane, K., Drareni, A., Hofmann, M., Becker, S., Gartner, A., Sagawe, A., 2011. Sands of West Gondwana: An archive of secular magmatism and plate interactions - A case study from the Cambro-Ordovician section of the Tassili Ouan Ahaggar (Algerian Sahara) using U-Pb-LA-ICP-MS detrital zircon ages. Lithos 123, 188–203.
Linnemann, U., Gerdes, A., Hofmann, M., Marko, L., 2014. The Cadomian Orogen: Neoproterozoic to Early Cambrian crustal growth and orogenic zoning along the periphery of the West African Craton-Constraints from U-Pb zircon ages and Hf isotopes (Schwarzburg Antiform, Germany). Precambrian Research 244, 236–278.
Ludwig, K.R., 2003. User's Manual for Isoplot 3.00: A Geochronological Toolkit for Microsoft Excel. p. 74.
Maleki, L., Rashidnejad-e-Omran, N., Hooshmandzadeh, A., 2019. Petrology, geochemistry and Sr-Nd isotopic composition of the metabasic rocks of Boneh shurow metamorphic complex, East of Saghand, Central Iran. Scientific Quarterly Journal, Geosciences 29 (196-185).
Meinhold, G., Morton, A.C., Avigad, D., 2013. New insights into peri-Gondwana paleogeography and the Gondwana super-fan system from detrital zircon U–Pb ages. Gondwana Research 23, 661–665.
Miskovic, A., Schaltegger, U., 2009. Crustal growth along a non-collisional cratonic margin: A Lu-Hf isotopic survey of the Eastern Cordilleran granitoids of Peru. Earth and Planetary Science Letters 279, 303–315.
Moghadam, H.S., Khademi, M., Hu, Z.C., Stern, R.J., Santos, J.F., Wu, Y.B., 2015. Cadomian (Ediacaran-Cambrian) arc magmatism in the ChahJam-Biarjmand metamorphic complex (Iran): Magmatism along the northern active margin of Gondwana. Gondwana Research 27, 439–452.
Moghadam, H.S., Li, X.H., Stern, R.J., Santos, J.F., Ghorbani, G., Pourmohsen, M., 2016. Age and nature of 560-520 Ma calc-alkaline granitoids of Biarjmand, northeast Iran: insights into Cadomian arc magmatism in northern Gondwana. International Geology Review 58, 1492–1509.
Moghadam, H.S., Griffin, W.L., Li, X.H., Santos, J.F., Karsli, O., Stern, R.J., Ghorbani, G., Gain, S., Murphy, R., O'Reilly, S.Y., 2017a. Crustal Evolution of NW Iran: Cadomian Arcs, Archean Fragments and the Cenozoic Magmatic Flare-Up. Journal of Petrology 58, 2143–2190.
Moghadam, H.S., Li, X.-H., Griffin, W.L., Stern, R.J., Thomsen, T.B., Meinhold, G., Aharipour, R., O'Reilly, S.Y., 2017b. Early Paleozoic tectonic reconstruction of Iran: Tales from detrital zircon geochronology. Lithos 268, 87–101.
Moghadam, H.S., Li, X.-H., Santos, J.F., Stern, R.J., Griffin, W.L., Ghorbani, G., Sarebani, N., 2017c. Neoproterozoic magmatic flare-up along the N. margin of Gondwana: The Taknar complex, NE Iran. Earth and Planetary Science Letters 474, 83–96.
Moghadam, H.S., Li, X.H., Griffin, W.L., Stern, R.J., Thomsen, T.B., Meinhold, G., Aharipour, R., O'Reilly, S.Y., 2017d. Early Paleozoic tectonic reconstruction of Iran: Tales from detrital zircon geochronology. Lithos 268, 87–101.
Moghadam, H.S., Li, X.H., Santos, J.F., Stern, R.J., Griffin, W.L., Ghorbani, G., Sarebani, N., 2017e. Neoproterozoic magmatic flare-up along the N. margin of Gondwana: The Taknar complex, NE Iran. Earth and Planetary Science Letters 474, 83–96.
Moghadam, H.S., Griffin, W.L., Kirchenbaur, M., Garbe-Schönberg, D., Zakie Khedr, M., Kimura, J.-I., Stern, R.J., Ghorbani, G., Murphy, R., O'Reilly, S.Y., Arai, S., Maghdour-Mashhour, R., 2018. Roll-Back, Extension and Mantle Upwelling Triggered Eocene Potassic Magmatism in NW Iran. Journal of Petrology 59, 1417–1465.
Moghadam, H.S., Corfu, F., Stern, R.J., Lotfi Bakhsh, A., 2019. The Eastern Khoy metamorphic complex of NW Iran: a Jurassic ophiolite or continuation of the Sanandaj–Sirjan Zone? Journal of the Geological Society. 176 (3), 517.
Momenzadeh, M., Heidari, E., 1995. Ore-hydrocarbon resources and alkaline magmatism of Late Proterozoic-Early Cambrian in Iran: A genetic interpretation. Carbonates and Evaporites 10, 79–88.
Nance, R.D., Murphy, J.B., Keppie, J.D., 2002. A Cordilleran model for the evolution of Avalonia. Tectonophysics 352, 11–31.
Nance, R.D., Gutierrez-Alonso, G., Keppie, J.D., Linnemann, U., Murphy, J.B., Quesada, C., Strachan, R.A., Woodcock, N.H., 2010. Evolution of the Rheic Ocean. Gondwana Research 17, 194–222.
Nutman, A.P., Mohajjel, M., Bennett, V.C., Fergusson, C.L., 2014. Gondwanan Eoarchean-Neoproterozoic ancient crustal material in Iran and Turkey: zircon U-Pb-Hf isotopic evidence. Canadian Journal of Earth Sciences 51, 272–285.
Paterson, S.R., Ducea, M.N., 2015. Arc Magmatic Tempos: Gathering the Evidence. Elements 11, 91–97.
Patiño Douce, A.E., 1997. Generation of metaluminous A-type granites by low-pressure melting of calc-alkaline granitoids. Geology 25, 743–746.
Patiño Douce, A.E., 1999. What do experiments tell us about the relative contributions of crust and mantle to the origin of granitic magmas? Geological society, london, special publications 168, 55–75.

Pearce, J.A., Peate, D.W., 1995. Tectonic Implications of the Composition of Volcanic Arc Magmas. Annual Review of Earth and Planetary Sciences 23, 251–285.
Pearce, J.A., Harris, N.B., Tindle, A.G., 1984. Trace element discrimination diagrams for the tectonic interpretation of granitic rocks. Journal of Petrology 25, 956–983.
Peccerillo, A., Taylor, S., 1975. Geochemistry of Upper Cretaceous volcanic rocks from the Pontic chain, northern Turkey. Bulletin of Volcanology 39, 557–569.
Pereira, M.F., Chichorro, M., Linnemann, U., Eguiluz, L., Silva, J.B., 2006. Inherited arc signature in Ediacaran and Early Cambrian basins of the Ossa-Morena Zone (Iberian Massif, Portugal): Paleogeographic link with European and North African Cadomian correlatives. Precambrian Research 144, 297–315.
Pereira, M.F., Linnemann, U., Hofmann, M., Chichorro, M., Sola, A.R., Medina, J., Silva, J.B., 2012. The provenance of Late Ediacaran and Early Ordovician siliciclastic rocks in the Southwest Central Iberian Zone: Constraints from detrital zircon data on northern Gondwana margin evolution during the late Neoproterozoic. Precambrian Research 192-95, 166–189.
Poore, H., White, N., Maclennan, J., 2011. Ocean circulation and mantle melting controlled by radial flow of hot pulses in the Iceland plume. Nature Geoscience 4, 558–561.
Rahmati-Ilkhchi, M., Faryad, S.W., Holub, F.V., Kosler, J., Frank, W., 2011. Magmatic and metamorphic evolution of the Shotur Kuh metamorphic complex (Central Iran). International Journal of Earth Sciences 100, 45–62.
Ramezani, J., Tucker, R.D., 2003. The Saghand Region, Central Iran: U-Pb geochronology, petrogenesis and implications for Gondwana Tectonics. American Journal of Science 303, 622–665.
von Raumer, J.F., 1998. The Palaeozoic evolution in the Alps: from Gondwana to Pangea. Geologische Rundschau 87, 407–435.
von Raumer, J.F., Stampfli, G.M., Borel, G., Bussy, F., 2002. Organization of pre-Variscan basement areas at the north-Gondwanan margin. International Journal of Earth Sciences 91, 35–52.
von Raumer, J.F., Stampfli, G.A., Bussy, F., 2003. Gondwana-derived microcontinents - the constituents of the Variscan and Alpine collisional orogens. Tectonophysics 365, 7–22.
von Raumer, J.F., Stampfli, G.M., Arenas, R., Martinez, S.S., 2015. Ediacaran to Cambrian oceanic rocks of the Gondwana margin and their tectonic interpretation. International Journal of Earth Sciences 104, 1107–1121.
Roberts, M.P., Clemens, J.D., 1993. Origin of High-Potassium, Calc-Alkaline, I-Type Granitoids. Geology 21, 825–828.
Rossetti, F., Nozaem, R., Lucci, F., Vignaroli, G., Gerdes, A., Nasrabadi, M., Theye, T., 2015. Tectonic setting and geochronology of the Cadomian (Ediacaran-Cambrian) magmatism in Central Iran, Kuh-e-Sarhangi region (NW Lut Block). Journal of Asian Earth Sciences 102, 24–44.
Ruban, D.A., Al-Husseini, M.I., Iwasaki, Y., 2007. Review of Middle East Paleozoic plate tectonics. Geoarabia 12, 35–56.
Rudnick, R.L., 1992. Restites, Eu Anomalies, and the Lower Continental-Crust. Geochimica Et Cosmochimica Acta 56, 963–970.
Rudnick, R.L., 1995. Making Continental-Crust. Nature 378, 571–578.
Saki, A., Moazzen, M., Oberhansli, R., 2011. P-T evolution of the Precambrian Metamorphic Complex, NW Iran: a study of metapelitic rocks. Geological Journal 46, 10–25.
Sanchez-Garcia, T., Quesada, C., Bellido, F., Dunning, G.R., del Tanago, J.G., 2008. Two-step magma flooding of the upper crust during rifting: The Early Paleozoic of the Ossa Morena Zone (SW Iberia). Tectonophysics 461, 72–90.
Schandl, E.S., Gorton, M.P., 2002. Application of high field strength elements to discriminate tectonic settings in VMS environments. Economic Geology 97, 629–642.
Sengor, A.M.C., Cin, A., Rowley, D.B., Shangyou, N., 1991. Magmatic Evolution of the Tethysides - a Guide to Reconstruction of Collage History. Palaeogeography Palaeoclimatology Palaeoecology 87, 411–440.
Sepidbar, F., Shafaii Moghadam, H., Zhang, L., Li, J.-W., Ma, J., Stern, R.J., Lin, C., 2019. Across-arc geochemical variations in the Paleogene magmatic belt of Iran. Lithos 344-345, 280–296.
Shabanian, N., Davoudian, A.R., Dong, Y.P., Liu, X.M., 2018. U-Pb zircon dating, geochemistry and Sr-Nd-Pb isotopic ratios from Azna-Dorud Cadomian metagranites, Sanandaj-Sirjan Zone of western Iran. Precambrian Research 306, 41–60.
Shafaii Moghadam, H., Li, Q.L., Griffin, W.L., Stern, R.J., Ishizuka, O., Henry, H., Lucci, F., O'Reilly, S.Y., Ghorbani, G., 2020. Repeated magmatic buildup and deep "hot zones" in continental evolution: The Cadomian crust of Iran. Earth and Planetary Science Letters 531.
Shakerardakani, F., Neubauer, F., Masoudi, F., Mehrabi, B., Liu, X.M., Dong, Y.P., Mohajjel, M., Monfaredi, B., Friedl, G., 2015. Panafrican basement and Mesozoic gabbro in the Zagros orogenic belt in the Dorud-Azna region (NW Iran): Laser-ablation ICP-MS zircon ages and geochemistry. Tectonophysics 647, 146–171.
Shakerardakani, F., Li, X.-H., Ling, X.-X., Li, J., Tang, G.-Q., Liu, Y., Monfaredi, B., 2019. Evidence for Archean crust in Iran provided by ca 2.7 Ga zircon xenocrysts within amphibolites from the Sanandaj–Sirjan zone. Zagros orogen. Precambrian Research 332.
Sisson, T.W., Salters, V., Larson, P., 2014. Petrogenesis of Mount Rainier andesite: Magma flux and geologic controls on the contrasting differentiation styles at stratovolcanoes of the southern Washington Cascades. Bulletin 126, 122–144.
Slama, J., Kosler, J., Condon, D.J., Crowley, J.L., Gerdes, A., Hanchar, J.M., Horstwood, M.S.A., Morris, G.A., Nasdala, L., Norberg, N., Schaltegger, U., Schoene, B., Tubrett, M.N., Whitehouse, M.J., 2008. Plesovice zircon - A new natural reference material for U-Pb and Hf isotopic microanalysis. Chemical Geology 249, 1–35.
Smedley, P.L., 1988. Trace-Element and Isotopic Variations in Scottish and Irish Dinantian Volcanism - Evidence for an Oib-Like Mantle Source. Journal of Petrology 29, 413–443.
Stampfli, G.M., 1996. The intra-alpine terrain: A paleotethyan remnant in the alpine variscides. Eclogae Geologicae Helvetiae 89, 13–42.
Stern, R.J., 1994. Arc assembly and continental collision in the Neoproterozoic East African Orogen: implications for the consolidation of Gondwanaland. Annual Review of Earth and Planetary Sciences 22, 319–351.
Stuart, C., Daczko, N., Piazolo, S., 2016. Local partial melting of the lower crust triggered by hydration through melt–rock interaction: an example from Fiordland. New Zealand, Journal of Metamorphic Geology.
Sun, S.-S., McDonough, W.S., 1989. Chemical and isotopic systematics of oceanic basalts: implications for mantle composition and processes. Geological society, london, special publications 42, 313–345.
Talbot, C., Aftabi, P., Chemia, Z., 2009. Potash in a salt mushroom at Hormoz island, Hormoz strait, Iran. Ore Geology Reviews 35, 317–332.
Tindle, A.G., Pearce, J.A., 1983. Assimilation and Partial Melting of Continental-Crust - Evidence from the Mineralogy and Geochemistry of Autoliths and Xenoliths. Lithos 16, 185–202.
Topuz, G., Gocmengil, G., Rolland, Y., Celik, O.F., Zack, T., Schmitt, A.K., 2013. Jurassic accretionary complex and ophiolite from northeast Turkey: No evidence for the Cimmerian continental ribbon. Geology 41, 255–258.
Topuz, G., Candan, O., Okay, A.I., von Quadt, A., Othman, M., Zack, T., Wang, J., 2020. Silurian anorogenic basic and acidic magmatism in Northwest Turkey: Implications for the opening of the Paleo-Tethys. Lithos 356, 105302.
Ustaomer, P.A., Ustaomer, T., Collins, A.S., Robertson, A.H.F., 2009. Cadomian (Ediacaran-Cambrian) arc magmatism in the Bitlis Massif, SE Turkey: Magmatism along the developing northern margin of Gondwana. Tectonophysics 473, 99–112.
Ustaomer, P.A., Ustaomer, T., Gerdes, A., Robertson, A.H.F., Collins, A.S., 2012. Evidence of Precambrian sedimentation/magmatism and Cambrian metamorphism in the Bitlis Massif, SE Turkey utilising whole-rock geochemistry and U-Pb LA-ICP-MS zircon dating. Gondwana Research 21, 1001–1018.
Vasyukova, O., Williams-Jones, A., 2019. Partial melting, fractional crystallisation, liquid immiscibility and hydrothermal mobilisation–A 'recipe'for the formation of economic A-type granite-hosted HFSE deposits. Lithos 356–357 105300.
Veiskarami, M., Sadeghian, M., Mingguo, M., Ghasemi, H., 2019. Petrology, geochemistry and dating of the Late Neoproterozoic metabasites of the Majerad metamorphic complex (SE Shahrood): One step for understanding the geodynamic evolutions of Iranian Gondawanan terranes. Iranian Journal of Crystallography and Mineralogy 27, 191–206.
Wang, R.R., Xu, Z.Q., Santosh, M., Yao, Y., Gao, L.E., Liu, C.H., 2016. Late Neoproterozoic magmatism in South Qinling, Central China: Geochemistry, zircon U-Pb-Lu-Hf isotopes and tectonic implications. Tectonophysics 683, 43–61.
Whalen, J.B., Currie, K.L., Chappell, B.W., 1987. A-type granites: geochemical characteristics, discrimination and petrogenesis. Contributions to Mineralogy and Petrology 95, 407–419.
Wiedenbeck, M., Alle, P., Corfu, F., Griffin, W., Meier, M., Oberli, F., Quadt, A.v., Roddick, J., Spiegel, W., 1995. Three natural zircon standards for U-Th-Pb, Lu-Hf, trace element and REE analyses. Geostandards newsletter 19, 1–23.
Winchester, J.A., Floyd, P.A., 1977. Geochemical discrimination of different magma series and their differentiation products using immobile elements. Chemical Geology 20, 325–343.
Wu, R.X., Zheng, Y.F., Wu, Y.B., Zhao, Z.F., Zhang, S.B., Liu, X.M., Wu, F.Y., 2006. Reworking of juvenile crust: Element and isotope evidence from Neoproterozoic granodiorite in South China. Precambrian Research 146, 179–212.
Yang, J.H., Wu, F.Y., Wilde, S.A., Chen, F., Liu, X.M., Xie, L.W., 2008. Petrogenesis of an alkali Syenite-Granite-Rhyolite suite in the Yanshan Fold and Thrust Belt, Eastern North China Craton: Geochronological, geochemical and Nd-Sr-Hf isotopic evidence for lithospheric thinning. Journal of Petrology 49, 315–351.
Zhang, L., Ren, Z.Y., Nichols, A.R.L., Zhang, Y.H., Zhang, Y., Qian, S.P., Liu, J.Q., 2014. Lead isotope analysis of melt inclusions by LA-MC-ICP-MS. Journal of Analytical Atomic Spectrometry 29, 1393–1405.
Zhao, Y.Y., Zheng, Y.F., Chen, F.K., 2009. Trace element and strontium isotope constraints on sedimentary environment of Ediacaran carbonates in southern Anhui, South China. Chemical Geology 265, 345–362.
Zindler, A., Hart, S., 1986. Chemical geodynamics. Annual Review of Earth and Planetary Sciences 14, 493–571.